



THE UNIVERSITY *of* EDINBURGH

Edinburgh Research Explorer

Bubble coalescence during pool boiling with different surface characteristics

Citation for published version:

Liu, J, Orejon Mantecon, D, Zhang, N, Terry, JG, Walton, AJ & Sefiane, K 2023, 'Bubble coalescence during pool boiling with different surface characteristics', *Heat Transfer Engineering*.
<https://doi.org/10.1080/01457632.2023.2191438>

Digital Object Identifier (DOI):

[10.1080/01457632.2023.2191438](https://doi.org/10.1080/01457632.2023.2191438)

Link:

[Link to publication record in Edinburgh Research Explorer](#)

Document Version:

Peer reviewed version

Published In:

Heat Transfer Engineering

General rights

Copyright for the publications made accessible via the Edinburgh Research Explorer is retained by the author(s) and / or other copyright owners and it is a condition of accessing these publications that users recognise and abide by the legal requirements associated with these rights.

Take down policy

The University of Edinburgh has made every reasonable effort to ensure that Edinburgh Research Explorer content complies with UK legislation. If you believe that the public display of this file breaches copyright please contact openaccess@ed.ac.uk providing details, and we will remove access to the work immediately and investigate your claim.



Bubble coalescence during pool boiling with different surface characteristics

Jionghui Liu^a, Daniel Orejon^a, Ningxi Zhang^a, Jonathan G. Terry^b, Anthony J. Walton^b,

Khellil Sefiane^{a*}

^a School of Engineering, Institute for Multiscale Thermofluids, University of Edinburgh,
Edinburgh, EH9 3FD, United Kingdom

^b School of Engineering, Institute for Micro and Nano Systems, University of Edinburgh,
Edinburgh, EH9 3FF, United Kingdom

Abstract

This work investigates the bubble dynamics during pool boiling from isolated cavities on a horizontal silicon substrate with three surface coatings, silicon oxide, Perfluorodecyltrichlorosilane, and silica nanoparticles. The experiments were conducted with FC-72 under various superheat degrees. In the case of vertical coalescence, coalescences at the boundary between the departed bubble and the subsequent nucleated bubble were observed and analysed. Vertical coalescence appears with lower superheat degrees on Perfluorodecyltrichlorosilane coated surfaces due to the faster initial bubble growth than on the other surfaces. However, the vertical coalescence has a limited effect on the bubble departure diameter, which is nearly kept constant at around 0.6 mm. In the case of horizontal coalescence, bubbles growing on the silica nanoparticles coated surface are able to coalesce for small cavity spacing with lower superheat degree than other surfaces. Coalescing bubbles from cavities spaced 0.50 mm apart can detach just after coalescence, while for a shorter spacing of 0.25 mm, bubbles remain attached to the surface and further growth is needed for their detachment. Based on the analysis of energy removal per unit of area, the optimal heat

transfer performance may be achieved when the cavities spacing is approximate to the single bubble departure diameter.

* Address correspondence to Prof. Khellil Sefiane, School of Engineering, Institute for Multiscale Thermofluids, University of Edinburgh, Edinburgh, EH9 3FD, U.K. E-mail: k.sefiane@ed.ac.uk

Introduction

Nucleate pool boiling plays a pivotal role in thermal systems, especially in addressing thermal management in electronic devices, including electric vehicles, photovoltaics and supercomputers [1, 2]. Compared with single-phase heat transfer, nucleate pool boiling can achieve much higher heat-transfer coefficients with minimum interface temperature difference due to the efficiency of phase-change heat transfer and the enhancement of the single-phase heat transfer by the convective motion of the bubble. Heat energy is not only directly removed by evaporation during bubble growth but also by the frequent rewetting of the surrounding fluid during bubble coalescence and departure [3-5]. One of the greatest challenges of nucleate pool boiling is to provide reliable and effective heat removal performance. Aiming to address this challenge, there is a growing body of literature that recognizes the importance of surface characteristics (roughness [6, 7], wettability [8, 9] and textures [10], etc.) and working conditions (orientation [11], working fluid [12] and pressure [13], etc.), enhancing the heat transfer ability and reliability of the phenomenon during boiling phase-change. However, many published studies are focused on the entire surface heat transfer performance, such as heat-transfer coefficient and critical heat flux (CHF) versus superheat degrees on the entire cooling area [14, 15]; while less work is focused on the bubble dynamics during nucleation, growth, coalescence and departure, which are intrinsic to boiling phase-change. Bubble growth and coalescence phenomenon are of great importance as they play a major role in enhancing heat transfer due to fluid rewetting the surface [16, 17]. Hence understanding the bubble coalescence behaviour needs more attention for the optimum development of surface topography with enhanced heat transfer characteristics.

For the single bubble behaviour, Bosnjaković *et al.* [18] firstly introduced a model that proposes that the latent heat utilised for the evaporation of the bubble comes from the thin superheated liquid

layer surrounding the bubble. Since then, many researchers have aimed to test this theory experimentally, and modified bubble growth equations have been proposed [19]. Thereafter Fritz [20] established the static force balance between surface tension and buoyancy forces to predict bubble departure diameter, which influences the boiling process, and several works have improved the theory under different working conditions [21]. Meanwhile, the bubble coalescence behaviour was further studied to determine the effect of bubble dynamics on heat transfer processes. Bubble coalescence can be classified into horizontal coalescence (coalescence between adjacent bubbles), vertical coalescence (coalescence between consecutive bubbles departing from the same cavity), and horizontal-vertical coalescence (coalescence between two adjacent rising bubbles) [16, 22]. Buyevich and Webbon [23] identified bubble coalescence as the primary critical mechanism leading to the boiling crisis and limiting the CHF.

On the one hand, vertical coalescence could result in the vapour column blocking the liquid contact with the wall, decreasing the effective area for heat transfer, and increasing the surface temperature difference locally. On the other hand, horizontal coalescence could increase the microlayer area and hence the energy removed from the surface with the consequent decrease in surface temperature difference. Bonjour *et al.* [16] studied the bubble coalescence phenomenon on a vertical heated surface with different artificial nucleation site arrangements. The cavity spacing ranged between 0.26 mm and 1.82 mm. The boiling curves for different nucleation site spacings were compared, and the occurrence of bubble coalescence was demonstrated to provide higher heat-transfer coefficients. In their work, the highest heat-transfer coefficients are obtained when the cavity spacing are between 1.05 mm and 1.5 mm (the average bubble departure diameter is between 1 mm and 1.25 mm). More recently, Coulibaly *et al.* [24-26] investigated the bubble coalescence under subcooled working fluid conditions and at constant wall temperature. As subcooling increases, i.e., the working fluid temperature lowers when compared to saturation, bubble coalescence induces

smaller bubble departure sizes and slower departure frequencies. It was found that bubble coalescence increases the rewetting of the heated surface, which causes heat flux fluctuations [24, 26]. However, fast coalescence (very quickly after nucleation) did not result in increasing heat fluxes between the surface and the bubbles as the liquid region was pushed away rather than creating an evaporating microlayer in Ref. 25 [25].

Focusing on the effect of surface characteristics on enhancing nucleate boiling heat transfer, numerous studies have attempted to investigate the bubble coalescence behaviour with different surface functionalities and structures. Sadaghiani *et al.* [17, 27] studied the effects of bubble coalescence on uncoated and coated (with a thin film of Teflon) surfaces comprising artificial cavities, i.e., hydrophilic and hydrophobic wettability configurations, respectively. Vertical coalescence was observed as the primary coalescence behaviour on the hydrophilic surface, whereas horizontal coalescence was the primary mechanism of bubble coalescence on the hydrophobic surface. A wide range of cavity pitch to size/diameter ratios between 2.5 and 40 was studied and compared. A critical cavity pitch to size/diameter ratio equal to or smaller than 10 was required to initiate the horizontal bubble coalescence. More recently, biophilic patterned surfaces have also been investigated in which hydrophobic spots/islands are created on a hydrophilic background [28]. According to the experimental results, the heat-transfer coefficient and CHF increased for hydrophobic to total surface area ratios up to 38.46%. Higher total surface to hydrophobic area ratios results in a decreasing trend in CHF and heat-transfer coefficient enhancement caused by earlier interaction of nucleated bubbles, thereby triggering the generation of a vapour blanket at lower wall superheat temperatures. Hutter *et al.* [2, 29, 30] investigated the bubble nucleation, growth and departure from artificial nucleation sites varying on different cavity parameters (10 μm cavity diameter and 80 μm cavity depth with 1.5 mm to 0.84 mm cavity spacing) on a silicon surface. The wall superheat degrees vary from 1 K to 16 K with system pressure changes between 0.5 bar and 1.0 bar. Hutter *et al.* [29] focused on vertical

coalescence, while horizontal coalescence was overlooked. The average bubble departure frequency and occurrence of vertical coalescence were found to increase with wall superheat degree and it was enhanced with decreasing system pressure [2]. Depending on the system pressure, consecutive vertical coalescence was reported for sub-atmospheric pressures under 0.5 bar at a high superheat degree, while intermittent vertical coalescence ensued under 1.0 bar pressure independently of the superheat degree. The equivalent volume of the coalescence bubbles revealed that the bottom bubble is always smaller than the initially departed one while the vapour volume remained nearly constant.

The research presented here builds upon an updated Hutter *et al.* [29] experimental rig and provides a systematic study of the effect of cavity spacing and surface wettability on bubble growth, coalescence and departure. More specifically, this paper focuses on a better understanding of both vertical and horizontal coalescence during nucleate pool boiling from 70 μm diameter artificial cavities on SiO, *Perfluorodecyltrichlorosilane* (FDTS) and Glaco coated surfaces. The cavity spacings vary from 0.25 mm to 1.50 mm, while the diameter and depth of the cavities remain the same. The occurrence of vertical and horizontal coalescence on the differently coated surfaces under different superheat and working pressure conditions was compared to find the effect of surface characteristics on the dynamics of bubble growth, coalescence and departure. Last, the performance of heat removal ability with bubble coalescence was compared to obtain the optimal cavity spacing as a function of the system conditions.

Experimental Setup and Procedure

Test rig

Schematics and snapshots of the experimental apparatus are shown in Fig. 1(a) and 1(b) respectively. Nucleate pool boiling was conducted in the boiling chamber, which has four integrated heaters located at the bottom of the chamber, represented in red in Fig. 1(a), to preheat the FC-72 liquid ($T_{sat} = 55.3 \text{ }^\circ\text{C}$ at $P = 1 \text{ bar}$, 3M^{TM}) to the saturation temperature. Two silicon-heating pads surround the boiling chamber were utilised allowing a uniform temperature of the FC-72 to be maintained within the chamber and minimising the heat losses to the environment. Two T-type thermocouples were used to measure the vapour and liquid temperature from the top and bottom of the boiling chamber with $\pm 0.1 \text{ K}$ accuracy. The pressure of the boiling chamber was measured and recorded by the digital pressure gauge with $\pm 0.1\%$ accuracy at room temperature. The boiling chamber pressure can be controlled and maintained between 0.5 bar to 3.0 bar by adjusting the flow rate and temperature of the cooling water in the external condenser, however the system pressure was kept at 1.25 bar for all experimental observation for a working fluid saturation temperature $T_{sat} = 64.2 \text{ }^\circ\text{C}$. The accuracy of thermal bath temperature control is $\pm 0.1 \text{ K}$.

Boiling surface

The boiling surface is a $50 \times 50 \text{ mm}^2$ silicon substrate with 12 micro-fabricated temperature sensors on the front side (as shown in Fig. 2(a)) and a micro-fabricated aluminium heater on the backside (as shown in Fig. 2(d)). Individual artificial cavities were etched in the centre of each temperature sensor, as shown in Fig. 2(b). The detailed micro-fabrication process can be found in the previous work of Hutter *et al.* [29, 30]. Each sensor has four connections, two that supply constant current through the sensor, while the remaining two measure the voltage and hence the cavity temperature by establishing a linear relationship between the sensor resistance and its temperature.

The temperature sensors were calibrated before and after experiments with the T-type thermocouples between 20 °C and 95 °C as shown in Fig. 3. The SEM image of the cavity shown in Fig. 2(c) gives the cavity diameter approximately to 70 µm and the depth of the cavity as around 110 µm. In order to investigate the bubble horizontal coalescence performance, the cavity spacings were arranged from 0.25 mm to 1.50 mm as shown in Fig. 4. The bubble departure diameter, D_d , for FC-72 at 1.25 bar pressure is around 0.60 mm so the dimensionless cavity spacing defined as the cavity spacing divided by the bubble departure diameter, S/D_d , ranges between 0.42 and 2.50. Horizontal bubble coalescence will happen at an early period (within in around 10 ms) in the presence of 0.25 mm cavity spacing ($S/D_d = 0.42$), while an optimum departure period was observed for 0.50 mm cavity spacing ($S/D_d = 0.83$). Horizontal bubble coalescence could not be observed with larger cavity spacings (from 1.00 mm to 1.50 mm cavities distances, i.e., S/D_d from 1.67 to 2.50) used to investigate isolate bubble growth and vertical bubble coalescence.

Three different surface coating procedures were used to change the surface wettability and topological characteristic. Plasma-Enhanced Chemical Vapour Deposition (PECVD) silicon oxide was coated onto the front surface of all the samples to protect the sensor. Some of these provided the SiO coated surfaces. Perfluorodecyltrichlorosilane was coated on top of the SiO via PECVD followed by oxygen plasma cleaning to provide the FDTS coated surfaces. The final set of samples was produced by dip-coating the SiO layer in Glaco TM Mirror Coat Zero (SOFT99, Japan) to give a uniform deposition of hydrophobic silica nanoparticles [31], providing the Glaco coated surfaces. These coating materials conferred the surface with different topology and wettability, as shown in Table 1. In summary, the SiO coated surface showed hydrophilic wettability with contact angles, θ_{ca} (°), for deionised water equal to 56°; and a surface roughness (R_a) of 37.8 nm; the FDTS coated surface achieved the lowest surface roughness, which was 5.5 nm, and a hydrophobic behaviour with contact angles, θ_{ca} (°), for deionised water equal to 103°; while the Glaco coated surface introduced

the highest surface roughness at 53.3 nm due to the presence of hydrophobic silica nanoparticles, which rendered the wettability super-hydrophobic with θ_{ca} above 160° for deionised water. Due to the very low liquid-gas surface tension of FC-72, the rendered contact angles θ_{ca} of FC-72 on these three coated surfaces are below 10° , also shown in Table 1.

The boiling test surface was then embedded on a PEEK (polyether ether ketone) polymer jig with spring probes to provide an electrical connection while holding the boiling surface section in the centre of the boiling chamber. Further details of the test section can be found in previous work [30]. A high precision multimeter (196 System DMM, Keithley Instruments Inc.) recorded the current from the temperature sensor and pressure data from the pressure transducer. The high-speed camera (Chronos 1.4 high speed camera with VZMTM - 450i lens) recorded the bubble growth between 1,000 fps and 15,000 fps. A trigger device was used to synchronize the high-speed camera and data acquisition (DAQ) system. The experimental process could be found in previous work [29].

Data reduction methods and uncertainty analysis

The change in bubble diameter with time, indicative of the bubble growth dynamics and the departure diameter, and the departure frequency were determined from high-speed video using the droplet analysis function in ImageJ software. The bubble equivalent diameter could be calculated based on the bubble area captured by the software as shown in Fig. 5(a) and the bubble departure height is the distance between the bottom point of the bubble area and the boiling surface as shown in Fig. 5(b). The measurement error was ± 2 px from image resolution, while the uncertainty of bubble diameter is about ± 0.1 mm, and the bubble departure frequency error was estimated to be ± 1 ms. All the thermocouples and temperature sensors have been calibrated in high accuracy thermal bath to ± 0.1 K. The heating power is controlled by adjustable power supply, and the input heat fluxes

are calculated by the input current and voltage. The experiment's heat fluxes are between 0.8 kW/m² and 21.4 kW/m².

Results and Discussion

Vertical bubble coalescence

First, we look at the effect of superheat degrees and surface characteristics on vertical bubble coalescence from artificial cavities with spacing equal or greater than 1.00 mm, i.e., greater than the bubble departure diameter, to rule out horizontal bubble coalescence. The effect of wall superheat is first investigated by using the Glaco coated surface as it showed the most prominent nucleation effect for lower superheat degrees. This allows for the best comparison of the effect of wall superheat and addresses the different vertical coalescing regimes as a function of the superheat degrees. After that, the effect of surface coating on vertical bubble coalescence is further investigated and analysed.

Effect of wall superheat degrees on vertical bubble coalescence

The wall superheat degree governs to some extent the amount of heat transferred from the surface to the liquid playing an important role in bubble nucleation, growth, departure, as well as whether there is a presence or absence of vertical bubble coalescence. To avoid interference from adjacent bubbles, only experiments between 1.00 mm and 1.50 mm cavity spacing were used for analysing vertical bubble coalescence.

By comparing the image sequences of bubble growth, vertical coalescence and departure, the boiling behaviour could be classified by the number of vertical coalescence occurrences for a departing bubble. The typical bubble growth on the Glaco coated surface at 1.25 bar with different superheat degrees can be observed in Fig. 6. At a low superheat degree of 4.2 K, isolated bubbles grow, until reaching the bubble departure diameter, D_d , and then depart from the surface without

vertical coalescence as shown in Fig. 6 (a). As the bubble reach the departure diameter, the bubble neck connecting the bubble and the cavity becomes thinner and breaks, which can be observed between -1 ms to 1 ms (0 ms is the moment that bubble departure from surface) in Fig. 6(a). Then, the top bubble rises because of buoyancy force, while there is vapour left in the cavity that continues to grow. We henceforth refer to the vapour left in the cavity after a bubble departure as a secondary vapour bubble or secondary remaining bubble. At such low superheat degrees, the growth of the secondary vapour bubble is not fast enough to reach and interact with the departed bubble. As the superheat degree increases, single-vertical coalescence ensues for a superheat degree of 7.7 K as presented in Fig. 6(b). Here, the first departing bubble merges with the fast-growing secondary vapour bubble resulting in a larger size bubble. Single-vertical coalescence and/or isolated bubble growth occur indistinctively when superheat degree is around 5.7 K. When increasing the superheat degree higher than 8.0 K, multi-vertical bubble coalescence occurs, as shown in Fig. 6(c). Here a tertiary vapour bubble (remaining on the surface after the coalescence of the first departing bubble with the fast-growing secondary vapour bubble) coalesces with the merged departed and secondary vapour bubbles. Multi-vertical coalescence phenomenon will occur more frequently as the input power increase, i.e., as the superheat degree increases.

Figure 7(a) compares the single bubble growth diameter and bubble departure distance (the distance between the bubble's bottom and the surface) for different superheat degrees on Glaco coated surfaces at 1.25 bar. The results obtained from the high-speed video show that the bubble departure distance (or bubble lift rate) is independent of the superheat degree, and shows a constant departure distance rate of nearly 0.086 mm/ms. It appears that the constant departure distance results as follows: bubbles growing from the same cavity presumably will be pinned to the cavity with an equal force, which needs to be overcome by the lifting or buoyancy force, which is in turn a function of the volume of the bubble. When looking into the bubble diameter growth, the secondary vapour bubble

remaining after the bubble neck breakage grows faster at higher superheat degree, especially for the initial period, as shown in Fig. 7(b). Vertical coalescence will happen on the surface when the remaining bottom bubble's diameter (or the bubble size) becomes larger than the departed bubble rise height; in other words, when the secondary bubble growth is faster than the departed bubble raising velocity. This is inferred from the open circle data points with departure diameters above the reported linear fitting for bubble lift distance in Fig. 7(b). For multi-vertical bubble coalescence, a second vertical coalescence event with a tertiary remaining bottom bubble happened at 4 ms. The fast growth of the tertiary vapour bubble coupled to the irregular shape of the raising merged bubble (comprised by the initial and secondary bubbles) at the vertical axis led to the second vertical coalescence reported in Fig. 6(c) between 3 ms and 6 ms.

The occurrence or absence of vertical bubble coalescence may in turn influence the bubble volume leaving the surface. Bubble volume is estimated by assuming axial symmetry around the vertical axis of the bubble. The average of ten consecutive vertical bubble departure volumes are shown in Fig. 8. In the case of 7.7 K and 10.2 K superheat degrees, subsequent secondary and tertiary bubble volumes for single- and for multi-vertical coalescence are also included and compared. The volume of the first departed bubble shows slight differences in both cases of single- and multi-vertical bubble coalescence. Meanwhile, the volume of the secondary bubble is rather constant implying that there is limited effect or variability on the following bubble growth. The volume of the bottom of the secondary vapour bubble is only about 2 % of the total departing volume (after departing and secondary vapour bubble coalescence) in Fig. 8(a). At a high superheat degree in the case of multi-vertical bubble coalescence, the volume of the tertiary vapour bubble doubles when compared to the secondary vapour bubble, as shown in Fig. 8(b).

The effect of superheat degrees on bubble departure diameter (first/departing bubble when vertical coalescence happened) in Fig. 9(a) shows that the bubble departure diameters are constrained

between 0.57 mm and 0.62 mm independent of the superheat degrees studied between 2 K and 10 K. Unlike the bubble behaviour observed in [Hutter *et al.* \[29\]](#) where the cavity diameter is 10 μm with 40 μm , 80 μm or 100 μm depth, the bubble departure diameter was found to increase with the wall superheat degrees. However, in the present case, the bubble departure diameter shows nearly constant values around 0.60 mm. Different bubble growth behaviour on smooth and improved surfaces were also observed by Chien *et al.* [32] and Chen *et al.*[33]. They compared the bubble behaviours on smooth tubes and enhanced tubes. In Chien's results, the bubble departure diameter showed a decrease with increasing heat flux on the enhanced surface, having 0.18 mm or 0.23 mm pore diameter and 0.75 mm or 1.5 mm pore pitch. In Chen's work, with higher heat flux, the bubble departure diameter increased on the smooth tube and decreased slightly on two kinds of enhanced tubes. The enhanced tubes have open slits with widths in the range of 0.01 mm to 0.1 mm and 0.05 mm to 0.2 mm, respectively. Bubble growth from very small cavities resembles bubble growth on a smooth surface. Typically, the bubble is inside the cavity and once the bubble diameter grows with sizes equal to the cavity diameter, since the buoyancy force is not strong enough to bring the bubble to depart from the surface, the bubble keeps growing, extending the bubble base diameter away from the cavity. This will lead to the formation of a microlayer under the bubble that affects the bubble growth [34, 35]. It seems in the cases of [Hutter *et al.* \[2\]](#) that the bubble departure diameter is controlled by the heating power and increases linearly with the superheat degree. However, for larger cavities, the bubble contact diameter is typically constrained to the cavity size and the bubble base diameter remains the same, especially after the initial growth period. Hence, for larger cavity sizes, the bubble departure diameter is mainly controlled by the cavity diameter with vapour generated around and inside the cavity or structure. When looking into the bubble departure frequency plotted in [Fig. 9\(b\)](#), this shows a nearly linear increase with increasing superheat degrees. While the bubble departure diameter is controlled by the cavity's diameter, the heating power affects the bubble growth

rate, which can be correlated with the linear increase in departure frequency. Additionally, it can be noted that the bubble departure frequency shows better linear relationship within the low superheat degree region under none-vertical bubble coalescence, i.e., $\Delta T_{sup} < 5$ K, while greater fluctuation in the bubble departure frequency arises as a consequence of the occurrence of single- and multi-vertical bubble coalescence, $\Delta T_{sup} > 5$ K.

Effect of surface characteristics on vertical bubble coalescence

Snapshots of the bubble growth and vertical bubble coalescence on SiO, FDTS and Glaco coated surfaces with wall superheat degrees of 6.0 K and 8.0 K are presented for the same timeframes in [Fig. 10](#) and [Fig. 11](#), respectively. The bubble departure behaviour is very similar on all three surfaces for either 6 K or 8 K superheat degrees. The top/first bubble departs from the surface after the ‘neck bridge’ between the bubble and the surface breaks due to the larger buoyance force pulling the first bubble upwards.

Despite the similar bubble departure behaviour, none-, single- and multi-vertical bubble coalescences occurred at different superheat ranges depending on the surface coating. Due to the super wettability of FC-72 fluid, the bubble shape of secondary and tertiary isolated bubbles and coalesced ones on all three kinds of surfaces are similar of the different superheat degrees. The bubble growth diameters and bubble departure heights are shown in [Fig. 12\(a\)](#) and [12\(b\)](#) for SiO and FDTS coated surfaces, respectively. It should be obvious that bubble growth rate during the initial period on the FDTS surface (larger slope of the bubble diameter curve) is faster than on the other coated surfaces causing earlier vertical bubble coalescence. The bubble departure height is similar on all three kinds of surfaces with a bubble lift rate of approximately 0.090 mm/ms compared to 0.086 mm/ms reported on Glaco.

A similar analysis to that shown in Fig. 8 for the Glaco coated surface where the volume of the first/departed, secondary bubble and its coalescence, and that of the final tertiary bubble and coalesced bubble (comprising the first, secondary and ternary bubbles) were carried out and represented for the other two coated surfaces in Fig. 13(a) for SiO and Fig. 13(b) for FDTS. The average volume of the coalesced bubble at 7.8 K superheat degree are 0.109 mm³, 0.112 mm³ and 0.113 mm³ for the Glaco, SiO and FDTS coated surfaces, respectively. The deviation between these coated surfaces is 0.004 mm³, which is less than 4 %. From these data, the volume of first/top bubble is about 96% to 98% of that of the first or second coalesced bubble independently. In these experiments, the contact area between the bubble and the surface increases during the initial period and then recedes upon bubble departure, as reported in earlier work [36]. The bubble contact diameter increases from 0.035 mm to around 0.080 mm during the initial period and then returns to 0.040 mm or a cavity diameter of 35 µm and a pressure of 1.25 bar [36]. The bubble contact area becomes equal to the cavity diameter on the three coated surfaces after the initial growth period. Hence, the volume as well as the bubble departure diameter can be considered independent of the surface finish and attributed to the cavity size as introduced earlier. However, the volume of the secondary/bottom vapour bubble on FDTS coated surface is ~~doubled twice, i.e., 100% larger~~, when compared with the secondary/bottom bubble on ~~the~~ SiO coated surface, ~~and~~. ~~It is~~ 33% larger when compared to the secondary/bottom vapour bubble volume on the Glaco coated surface.

The bubble departure diameter on the SiO and FDTS coated surfaces is shown in Fig. 14(a) and Fig. 14(b), respectively. In contrast, the same results for the Glaco coated surface can be found in Fig. 9(a) for comparison. As in the case of the Glaco coated surface, the average bubble departure diameter is independent of the superheat degree with an average bubble departure diameter of 0.59 mm for SiO and 0.61 mm for the FDTS coated surfaces compared to 0.60 mm for the Glaco coated surface. Hence, it can be concluded that in the presence of larger cavity diameters (70 µm), the

difference in wettability and/or roughness imposed by the different coatings do not affect the bubble departure diameter for the range of superheat degree studied in this work.

The bubble departure frequency on SiO and FDTS coated surfaces, which is shown in Fig. 15(a) and 15(b), respectively, while results for Glaco coated surface were introduced in Fig. 9(b). It is found that single- and multi-vertical bubble coalescence ensues earlier on the FDTS coated surface than on Glaco or SiO coated surfaces. On FDTS coated surface, single-vertical coalescence appears for superheat degrees as low as 3.8 K, which is nearly 2.0 K lower than on the other two coated surfaces (5.7 K on Glaco and 5.8 K on SiO). Furthermore, on FDTS coated surface, multi-vertical coalescence ensues at a lower superheat degree of 7.7 K when compared to Glaco coated surface at 8.0 K and SiO at 8.7 K.

Bubble horizontal coalescence

Having examined bubble growth from isolated cavities, we now consider the bubble growth and horizontal bubble coalescence behaviours paying special attention to the cavity spacing. The different horizontal bubble coalescence and departure performance for 0.25 mm and 0.50 mm cavity spacings on the Glaco coated surface under various superheat degrees are considered. The horizontal bubble coalescences on the different coated surfaces are then estimated and compared in the presence and absence of horizontal coalescence.

Effect of cavity spacing on horizontal bubble coalescence

Horizontal bubble coalescence with 0.25 mm and 0.50 mm cavity spacings are shown in Fig. 16(a) and 16(b), respectively. Initially, two isolated bubbles nucleate and grow from each cavity, regardless of the cavity spacing. The bubbles keep growing until they are close enough to coalesce/merge into a single larger bubble. However, depending on the cavity spacing, two different

kinds of coalescence behaviour were identified. With spacings of 0.25 mm, two single bubbles coalesced into a larger bubble and the coalesced bubble kept growing while the base bubble diameter engulfed both cavities, i.e., the base bubble diameter **and hence bubble pinning** becomes considerably larger than during single bubble growth. Then, the coalesced bubble continues growing until it is large enough for buoyancy forces to overcome surface tension forces or adhesion forces, at which point it departs from the surface. **On one hand,** when looking in more detail into how bubbles depart after coalescing on the shortest of the cavity distance of 0.25 mm, a clear vapour bridge/neck underneath the merged bubble and between the two cavities can be observed during the departure period as shown in **Fig. 16(a)** for timeframes between 44 ms and 46 ms. Thereafter, the vapour bridge/neck connecting one of the cavities, i.e., the right cavity, breaks, leaving a small vapour bubble on the right cavity while the coalesced bubble hangs over the left cavity as how in **Fig. 16(a)** at 47 ms and finally it detaches while some vapour remains in the left cavity. On the other hand, for larger cavity spacing, i.e., 0.50 mm, coalesced/merged bubbles depart from the surface within few milliseconds after bubble coalescence occurs as shown in **Fig. 16(b)** for timeframes between 36 ms and 39 ms. **For 0.50 mm spacing, coalescence and departure happened within only 3 ms.**

Observations of bubble nucleation, growth and departure for Glaco coated with 0.75 mm, 1.00 mm and 1.25 mm cavity spacings are shown in **Fig. 17**, which further confirm the absence of coalescence for these cavity spacings. From these observations, the adjacent bubble growth does not show any clear effect during the growth period and there is no interaction between neighbouring bubbles during departure.

The bubble growth diameter for single and coalesced bubbles for cavity distances of 0.25 mm and 0.50 mm are presented in **Fig. 18(a) and 18(b)**, respectively. Single bubble growth from the left cavity is represented as black symbols, bubble growth from the right cavity as red symbols, isolated bubble growth as purple symbols, while coalesced bubble growth is represented as blue symbols. All

bubble growths were measured under similar superheat degree for 1.25 mm cavity spacings. It is worth noting the continuity in the volume and the continuous bubble growth between green and blue symbols. Green symbols add up the right and left bubble volumes before coalescence. These results show that bubble coalescence does not affect single and merged bubbles growth dynamics. This is possibly due to the high wetting characteristics of FC-72. The coalescence of the bubbles does not result in any obviously change off the contact line length (solid/liquid/vapour triple phase contact line), which is where vaporization mainly takes place during the bubble growth process [5].

The bubble departure diameter and departure frequency at different superheat degrees in the presence of horizontal bubble coalescence for different cavity spacing of 0.25 mm and 0.50 mm on Glaco coated surface are shown in Fig. 19(a) and 19(b), respectively. The bubble departure diameter and the bubble departure frequency for larger cavities distances in the absence of horizontal bubble coalescence are also shown in Fig. 19(a) and 19(b). Horizontal bubble coalescence occurs for 0.25 mm and 0.50 mm cavity spacing for superheat degree higher than 4.0 K. The larger bubble departure diameter compared with the other three cavity spacings, where horizontal coalescence could not be observed, is rather noteworthy. The 0.50 mm cavity spacing achieves the highest bubble departure diameter with a value of around 0.78 mm, and decreases to around 0.72 mm for 0.25 mm cavity spacing. However, when the merged bubble departure diameter is taken into account and compared to a single bubble departure from two cavities, the departure diameter in the presence of horizontal coalescence is smaller than that of an isolated bubble departure. This can be seen in Fig. 19(a), where the red and black points are lower than the purple dotted line representing the equivalent diameter of two bubbles with the departing size of approximately 0.60 mm. Fig. 19(b) shows a nearly linear increase in frequency with superheat degrees across the different cavity spacings. When comparing the same superheat conditions, the average departure frequency for 0.50 mm cavity spacing was slightly higher than for the other conditions. This is supported by the departure from the surface upon

coalescence shown in Fig. 16(b). While for the 0.25 mm cavity distance case, the average bubble departure frequency is lower than for the other conditions, which likely contributes to the merged bubbles' larger contact area that leads to a more extended bubble growth period after coalescence. When looking into larger cavity distance, the departure frequency difference between 0.75 mm to 1.25mm cavity spacings are minimal supporting the earlier statement that single bubble growth of adjacent bubbles does not disturb or influence the bubble growth dynamics, the bubble departure diameter or the bubble departure frequency. For these large cavity spacings, the bubble departure diameter keeps a nearly constant value of around 0.60 mm for superheat degrees ranging from 2 K to 10 K, as was the case for the 0.75 mm and 1.25 mm cavity spacing, as shown in Fig. 9(a) and Fig. 14.

Effect of surface characteristics on horizontal bubble coalescence

The horizontal bubble coalescence has been investigated on the FDTS, and SiO coated surfaces. Figure 20 shows that horizontal bubble coalescence takes place on all three coated surfaces under various superheat degrees with 0.25 mm cavity spacing. Bubble coalescence is observed on the Glaco coated surface for superheat degrees higher than 4.0 K. However, horizontal bubble coalescence did not ensue on the other two surfaces with very low superheat degree. In the case of the FDTS coated surface, superheat degrees higher than 10 K are needed for horizontal coalescence to happen, while superheat degrees as high as 16 K were required in the case of the SiO coated surface. The bubble dynamics could not be analysed under high superheat degrees above 16 K due to the convection taking place within the chamber leading to loss of image quality.

Energy removal analysis

From the above results, the energy removal per unit of area has been estimated and compared in the presence and absence of horizontal bubble coalescence. The energy removal Q_e (W) per unit area A (m^2) referred to as q_e (W/m^2) can be estimated from the bubble volume leaving the surface using Equation (1):

$$q_e = Q_e/A = (\pi D_d^3 \rho_g f h_{fg}/6)/(\pi D_d^2/4) = 2D_d \rho_g h_{fg} f/3 \quad (1)$$

where D_d is the bubble departure diameter (mm), ρ_g is the density of bubble gas (kg/m^3), f is the departure frequency (Hz), and h_{fg} is the latent heat of vaporization (J/kg). The comparison of the energy removal per unit area for different cavities distance versus superheat degrees is shown in Fig. 21. It is worth noting that the heat flux for the 0.75 mm to 1.25 mm cavities distance cases are similar and agree quantitatively well with the previous data obtained by Hutter *et al.* [29], with 10 μm cavity diameter and 40 to 100 μm cavity depth. However, the hear flux in the case of 0.25 mm and 0.50 mm cavity spacings are higher than for other conditions owing to the bubble horizontal coalescence. So, the arrangement and density of cavity/nucleation sites on the surface could affect the overall heat transfer performance. The optimal design is to ensue more frequency of bubbles nucleating on the surface as well as a faster departure frequency.

Conclusion

The present paper studies vertical and horizontal FC-72 bubble coalescence from 70 μm diameter isolated cavities with defined spacing between cavities on a horizontal silicon substrate. The effect of surface wettability and outermost layer characteristics have been compared by treating the surface with three different surface coatings. The bubble behaviour under various superheat degrees and different cavity spacings, have been then compared and analysed. The following conclusions have been drawn from this work:

Vertical coalescence has a minimal effect on the bubble departure diameter since the bottom bubble volume is only about 2 % of that of the top bubble volume. The bubble average departure diameter is approximately 0.60 mm independently of the coating and superheat degrees, while the bubble departure frequency shows a nearly linear increase with increasing superheat degree. This is possible due to the very low liquid-gas surface tension properties of the FC-72.

In the case of vertical bubble coalescence, the FDTS coated surface could achieve earlier vertical bubble coalescence compared with Glaco and SiO coated surface. This is because the non-wetting and smooth surface finish of the FDTS coated surface has more noticeable effect on the faster initial growth period of the bottom bubble. For low superheat degree, single-vertical coalescence occurs on the FDTS coated surface at 3.8 K, which is nearly 2 K lower than in the case of the other coated surfaces. For high superheat degree, multi-vertical coalescence is observed for the FDTS coated surface at 7.7 K, while for Glaco coated surface it ensued at 8.0 K and at 8.8 K for the SiO coated surface.

In the case of horizontal bubble coalescence, the Glaco coated surface resulted in coalescence for low superheat degree on both 0.25 mm and 0.50 mm cavity spacings. By contrast, it is 6.0 K lower than horizontal coalescence on the FDTS and/or on SiO coated surfaces, which require superheat degrees above 10 K.

In addition, the bubble departure dynamics on the Glaco coated surface differ when comparing the different cavity spacings. In the experiments, merged bubble departed from the surface following a coalescence event on 0.50 mm cavity spacing whereas the merged bubble remained attached and growing after coalescence on 0.25 mm cavity spacing ones.

Horizontal bubble coalescence does not affect single and merged bubble growth. A single bubble in each cavity follows the isolated bubble growth regime before coalescence. The merged bubble growth follows the trend by adding right and left bubble volumes together. The coalescence of the adjacent bubble mainly affects the bubble departure diameter and departure frequency.

Finally, from the results of the heat removed ability per unit area, the optimal heat transfer performance could be achieved when the cavities distance is approximately equal to the single bubble departure diameter. It is hypothesised that for a certain surface area, the optimal cavity density and arrangement could enable more bubbles to be generated on the surface with a faster departure frequency, which could result in more efficient cooling.

Nomenclature

A	area, m ²
CHF	critical heat flux, W/m ²
DAQ	data acquisition
D_{cavity}	artificially cavity diameter, mm
D_d	bubble departure diameter, mm
f	departure frequency, Hz
FDTS	Perfluorodecyltrichlorosilane
h_{fg}	latent heat of vaporisation, J/kg
P	boiling chamber pressure, bar
PECVD	plasma-enhanced chemical vapour deposition
PEEK	polyether ether ketone
R_a	surface roughness, nm
T	temperature, °C
Q_e	evaporative heat energy, W
q_e	evaporative heat flux per unit area, W/m ²
S	two cavities spacing, mm
SEM	scanning electron microscope
V	bubble volume, mm ³

Greek symbols

ρ_g	vapour density, kg/m ³
θ_{ca}	contact angle, °
ΔT_{sup}	superheat degree, K

Subscripts

<i>ave</i>	average value
<i>top</i>	top bubble
<i>bot</i>	bottom bubble
<i>coa</i>	coalescence bubble
<i>sat</i>	saturation

Acknowledgement

We acknowledge support from EPSRC of the U.K. (EP/S019588/1). The experimental surfaces were manufactured on silicon wafers at the University of Edinburgh's cleanroom facilities housed in the Scottish Microelectronics Centre.

References

- [1] J. T. Cieśliński and T. Z. Kaczmarczyk, “Pool boiling of water- Al_2O_3 and water-Cu nanofluids outside porous coated tubes,” *Heat Transfer Eng.*, vol. 36, no. 6, pp. 553–63, 2015. DOI: 10.1080/01457632.2014.939046.
- [2] C. Hutter *et al.*, “Vertical coalescence during nucleate boiling from a single artificial cavity,” *Exp. Therm. Fluid Sci.*, vol. 51, 2013, pp. 94–102, 2013. DOI: 10.1016/j.expthermflusci.2013.07.005.
- [3] M. M. Rahman and M. Matthew, “Boiling enhancement on nanostructured surfaces with engineered variations in wettability and thermal conductivity,” *Heat Transfer Eng.*, vol. 38, no. 14-15, pp. 1285–95, 2017. DOI: 10.1080/01457632.2016.1242961.
- [4] P. I. Shyamkumar, S. Singh and A. Srivastava, “Numerical investigation of nucleate pool boiling heat transfer for different superheat conditions,” *Heat Transfer Eng.*, vol. 43, no. 1, pp. 83–100, 2021. DOI: 10.1080/01457632.2020.1844450.
- [5] J. Kim, “Review of nucleate pool boiling bubble heat transfer mechanisms,” *Int. J. Multiphase Flow*, vol. 35, no. 12, pp. 1067–1076, 2009. DOI: 10.1016/j.ijmultiphaseflow.2009.07.008.
- [6] J. Kim *et al.*, “Effect of surface roughness on pool boiling heat transfer at a heated surface having moderate wettability,” *Int. J. Heat Mass Transfer*, vol. 101, pp. 992–1002, 2016. DOI: 10.1016/j.ijheatmasstransfer.2016.05.067.
- [7] B. J. Jones, J. P. McHale and S. V. Garimella, “The influence of surface roughness on nucleate pool boiling heat transfer,” *J. Heat Transfer*, vol. 131, no. 12, pp. 1–14, 2009. DOI: 10.1115/1.3220144.
- [8] J. Shi, X. Jia and D. Feng, “Wettability effect on pool boiling heat transfer using a multiscale copper foam surface,” *Int. J. Heat Mass Transfer*, vol. 146, 118726, 2020. DOI: 10.1016/j.ijheatmasstransfer.2019.118726.

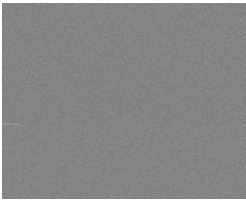
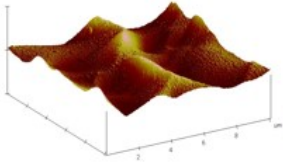
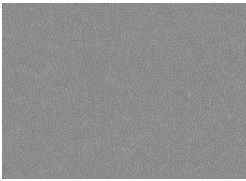
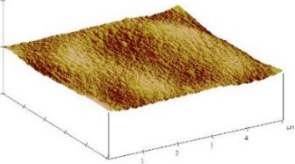
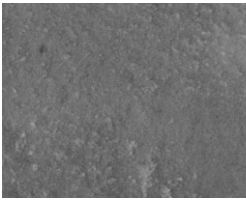
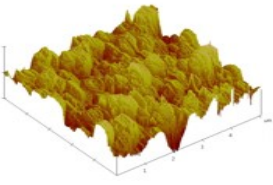
- [9] H. T. Phan, N. Caney and P. Marty, “Surface wettability control by nanocoating: the effects on pool boiling heat transfer and nucleation mechanism,” *Int. J. Heat Mass Transfer*, vol. 52, no. 23, pp. 5459–5471, 2009. DOI: 10.1016/j.ijheatmasstransfer.2009.06.032.
- [10] Y. Hwasung, K. Sridharan and M. Corradini, “Bubble dynamics in pool boiling on nanoparticle-coated surfaces.” *Heat Transfer Eng*, vol. 36, no. 12, pp. 1013–27, 2015. DOI: 10.1080/01457632.2015.979116.
- [11] S. M. Kwark, M. Amaya and R. Kumar, “Effects of pressure, orientation, and heater size on pool boiling of water with nanocoated heaters,” *Int. J. Heat Mass Transfer*, vol. 53, no. 23, pp. 5199–5208, 2010. DOI: 10.1016/j.ijheatmasstransfer.2010.07.040.
- [12] E.C. Forrest, L. Hu, J. Buongiorno and T. J. McKrell, “Pool boiling heat transfer performance of a dielectric fluid with low global warming potential,” *Heat Transfer Eng.*, vol. 34, no. 15, 2013, pp. 1262–77, 2013. DOI: 10.1080/01457632.2013.793103.
- [13] Y. Zhang, J. Zhao and J. Wei, “Nucleate pool boiling heat transfer on a micro-pin-finned surface in short-term microgravity,” *Heat Transfer Eng.*, vol. 38, no. 6, pp. 594–610, 2017. DOI: 10.1080/01457632.2016.1200377.
- [14] G. Liang and I. Mudawar, “Pool boiling critical heat flux (CHF)–Part 1: Review of mechanisms, models, and correlations,” *Int. J. Heat Mass Transfer*, vol. 117, pp. 1352–1367, 2018. DOI: 10.1016/j.ijheatmasstransfer.2017.09.134.
- [15] G. Liang and I. Mudawar, “Review of pool boiling enhancement by surface modification,” *Int. J. Heat Mass Transfer*, vol. 128, pp. 892–933, 2019. DOI: 10.1016/j.ijheatmasstransfer.2018.09.026.
- [16] J. Bonjour, M. Clausse and M. Lallemand, “Experimental study of the coalescence phenomenon during nucleate pool boiling,” *Exp. Therm. Fluid Sci.*, vol. 20, no. 3, pp. 180–187, 2000, DOI: 10.1016/S0894-1777(99)00044-8.

- [17] A. K. Sadaghiani *et al.*, “Effects of bubble coalescence on pool boiling heat transfer and critical heat flux—A parametric study based on artificial cavity geometry and surface wettability,” *Int. J. Heat Mass Transfer*, vol. 147, 118952, 2020. DOI: 10.1016/j.ijheatmasstransfer.2019.118952.
- [18] F. Bosnjaković. “Verdampfung und Flüssigkeitsüberhitzung,” *Technische Mechanik und Thermodynamik*, vol.1, pp. 358-362, 1930. DOI: 10.1007/BF02640224.
- [19] N. Zuber, “The dynamics of vapor bubbles in nonuniform temperature fields,” *Int. J. Heat Mass Transfer*, vol. 2, no. 1, pp. 83–98, 1961. DOI: 10.1016/0017-9310(61)90016-3.
- [20] W. Friz, “Maximum volume of vapor bubbles,” *Physic. Zeitschz*, vol. 36, pp. 379-354, 1935.
- [21] J. Zhou, P. Xu and B. Qi, “Effects of micro-pin-fins on the bubble growth and movement of nucleate pool boiling on vertical surfaces.” *Int. J. Therm. Sci.*, vol. 171, 107186, 2022, DOI: 10.1016/j.ijthermalsci.2021.107186.
- [22] L. Zhang and M. Shoji, “Nucleation site interaction in pool boiling on the artificial surface,” *Int. J. Heat Mass Transfer*, vol. 46, no. 3, pp. 513-522, 2003. DOI: 0.1016/S0017-9310(02)00291-0.
- [23] Y. A. Buyevich and B. W. Webbon, “The isolated bubble regime in pool nucleate boiling,” *Int. J. Heat Mass Transfer*, vol. 40, no. 2, pp. 365–377, 1997. DOI: 10.1016/0017-9310(96)00097-X.
- [24] A. Coulibaly, X. Lin and J. Bi, “Bubble coalescence at constant wall temperatures during subcooled nucleate pool boiling,” *Exp. Therm. Fluid Sci.*, vol. 44, pp. 209–218, 2013. DOI: 10.1016/j.expthermflusci.2012.06.010.
- [25] A. Coulibaly, J. Bi and X. Lin, “Effect of bubble coalescence on the wall heat transfer during subcooled pool boiling,” *Int. J. Therm. Sci.*, vol. 76, pp. 101–109, 2014. DOI: 10.1016/j.ijthermalsci.2013.08.019.

- [26] A. Coulibaly, J. Bi and D. M.Christopher, “Experimental investigation of bubble coalescence heat transfer during nucleate pool boiling,” *Exp. Therm. Fluid Sci.*, vol. 104, pp. 67–75, 2019. DOI: 10.1016/j.expthermflusci.2019.01.024.
- [27] A. K. Sadaghiani, A. R. Motezakker and A. V. Özpınar, “Pool boiling heat transfer characteristics of inclined pHEMA-coated surfaces,” *J. Heat Transfer*, vol. 139, no. 11, 2017. DOI: 10.1115/1.4036651.
- [28] A. R. Motezakker *et al.*, “Optimum ratio of hydrophobic to hydrophilic areas of biphilic surfaces in thermal fluid systems involving boiling,” *Int. J. Heat Mass Transfer*, vol. 135, pp. 164–74, 2019. DOI: 10.1016/j.ijheatmasstransfer.2019.01.139.
- [29] C. Hutter *et al.*, “Experimental pool boiling investigations of FC-72 on silicon with artificial cavities and integrated temperature microsensors,” *Exp. Therm. Fluid Sci.*, vol. 34, no. 4, pp. 422–433, 2010. DOI: 10.1016/j.expthermflusci.2009.03.010.
- [30] C. Hutter *et al.*, “Nucleation site interaction between artificial cavities during nucleate pool boiling on silicon with integrated micro-heater and temperature micro-sensors,” *Int. J. Heat Mass Transfer*, vol. 55, no. 11-12, pp. 2769–78, 2012. DOI: 10.1016/j.ijheatmasstransfer.2012.02.01.
- [31] A. Rajappan and G. H.McKinley, “Cooperative drag reduction in turbulent flows using polymer additives and superhydrophobic walls,” *Physical Review Fluids*, vol. 5, no. 11, 2020. DOI: 10.1103/PhysRevFluids.5.114601.
- [32] L. H. Chien and R. L. Webb, “Measurement of bubble dynamics on an enhanced boiling surface,” *Exp. Therm. Fluid Sci.*, vol. 16, no. 3, pp. 177-186, 1998. DOI: 10.1016/S0894-1777(97)10017-6.

- [33] Y. Chen, M. Groll and R. Mertz, “Bubble dynamics of boiling of propane and iso-butane on smooth and enhanced tubes,” *Exp. Therm. Fluid Sci.*, vol. 28, no. 2, pp. 171–78, 2004. DOI: 10.1016/S0894-1777(03)00036-0.
- [34] Y. Sun *et al.*, “Pool boiling performance and bubble dynamics on microgrooved surfaces with reentrant cavities,” *Appl. Therm. Eng.*, vol. 125, pp. 432–42, 2017. DOI: 10.1016/j.applthermaleng.2017.07.044.
- [35] M. G. Cooper and A. J. P. Lloyd, “The microlayer in nucleate pool boiling,” *Int. J. Heat Mass Transfer*, vol. 12, no. 8, pp. 895–913, 1969. DOI: 10.1016/0017-9310(69)90154-9.
- [36] J. Liu *et al.*, “Effect of cavity diameter and pressure on pool boiling bubble dynamics,” presented at the 17th U.K. Heat Transfer Conference, Manchester, U.K., April 4-6 2022.

Table 1. Surface characteristic

	SEM Scanning	AFM Scanning	Contact Angle	
			DI water	FC-72
SiO		$Ra = 37.8 \text{ nm}$ 	$\theta_{ca} = 56^\circ$	$\theta_{ca} < 10^\circ$
FDTS		$Ra = 5.5 \text{ nm}$ 	$\theta_{ca} = 103^\circ$	$\theta_{ca} < 10^\circ$
Glaco		$Ra = 53.3 \text{ nm}$ 	$\theta_{ca} = 162^\circ$	$\theta_{ca} < 10^\circ$

List of Figure Captions

- Figure 1. (a) Schematically overview and (b) snapshots of the experimental setup.
- Figure 2. (a) Boiling surface temperature sensor side; (b) temperature sensor micrograph; (c) cavity SEM photo; (d) boiling surface heater side;
- Figure 3. Calibrated curve between the resistance of temperature sensors and the temperature.
- Figure 4. Schematic diagram of cavity spacings, S (mm), dimensionless cavity spacing, S/D_d , and effect on bubble growth.
- Figure 5. (a) Definition of bubble diameter and (b) definition of bubble departure distance.
- Figure 6. Bubble departure snapshots for different wall superheat degrees with 1.00 mm cavity spacing (a) none-vertical coalescence at $\Delta T_{sup} = 4.2$ K; (b) single-vertical coalescence at $\Delta T_{sup} = 7.7$ K; (c) multi-vertical coalescence at $\Delta T_{sup} = 10.2$ K on Glaco coated surface at 1.25 bar with $t = 0$ ms as the time right before the bubble neck breaks and the first/larger bubble departs.
- Figure 7. Single bubble growth diameter (mm) and bubble departure distance (mm) versus time (ms) for different superheat degree (K) on Glaco coated surface with 1.00 mm cavity spacing (a) whole period and (b) initial period as the grey area in (a).
- Figure 8. The average bubble volume (mm^3) during (a) single-vertical coalescence of the different bubbles (first/departing, secondary bubble and coalesced bubble) at $\Delta T_{sup} = 7.7$ K and (b) multi-vertical coalescence of the different bubbles (first/departing, secondary bubble, tertiary bubble and coalesced bubble) at $\Delta T_{sup} = 10.2$ K on Glaco coated surface for a total of ten different pairs of bubbles with 1.00 mm cavity spacing.
- Figure 9. (a) Bubble departure diameter (mm) and (b) bubble departure frequency (Hz) versus superheat degree (K) on Glaco coated surface at 1.25 bar with 1.00 mm to 1.50 mm cavity spacing.
- Figure 10. Bubble departure snapshots with different coated surfaces and 1.00 mm cavity spacing. (6.0 K superheat degree)
- Figure 11. Bubble departure snapshots with different coated surfaces and 1.00 mm cavity spacing. (8.0 K superheat degree)

Figure 12. Single bubble growth diameter (mm) and bubble departure height (mm) versus time (ms) with different superheat degree on (a) SiO coated surface and (b) FDTS coated surface with 1.00 mm cavity spacing.

Figure 13. The average bubble volume (mm^3) during vertical coalescence of first/departing, secondary bubble and coalesced bubble for a total of ten different pairs of bubbles with 1.00 mm cavity spacing at (a) $\Delta T_{sup} = 7.8$ K on SiO coated surface and (b) $\Delta T_{sup} = 7.8$ K on FDTS coated surface.

Figure 14. Bubble departure diameter (mm) versus superheat degree (K) with 1.00 mm to 1.50 mm cavity spacings on (a) SiO coated surface and (b) FDTS coated surface.

Figure 15. Bubble departure frequency (Hz) versus superheat degree (K) with 1.00 mm to 1.50 mm cavity spacings on (a) SiO coated surface and (b) FDTS coated surface.

Figure 16. The entire bubble horizontal coalescence cycle on the Glaco coated surface with (a) 0.25 mm cavity spacing and (b) 0.50 mm cavity spacing at approximately 4.7 K superheat degree.

Figure 17. The bubble growth behaviour for 0.75mm, 1.00mm and 1.25 mm cavity spacings on the Glaco coated surface at approximately 4.5 K superheat degree.

Figure 18. The single and coalesced bubble growth diameter (mm) versus time (ms) for (a) 0.25 mm cavity spacing and (b) 0.50 mm cavity spacing at approximately 4.7 K superheat degree

Figure 19. The bubble (a) departure diameter (mm) and (b) departure frequency (Hz) versus superheat degree (K) for different cavity spacings on Glaco coated surface.

Figure 20. Bubble coalescence performance versus superheat degree (K) and surface coating with 0.25 mm cavity spacing.

Figure 21. Energy removal per unit of area q_e (kW/m^2) versus superheat degree (K) considering by evaporation.

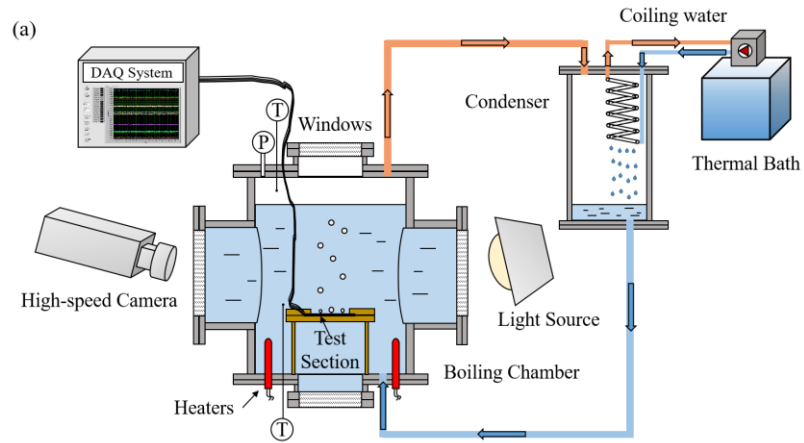


Figure 1. (a) Schematically overview and (b) snapshots of the experimental setup.

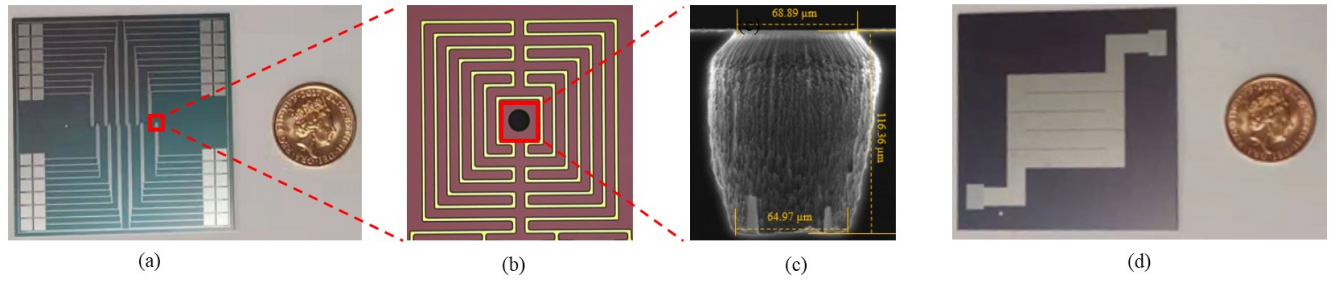


Figure 2. (a) Boiling surface temperature sensor side; (b) temperature sensor micrograph; (c) cavity SEM photo; (d) boiling surface heater side;

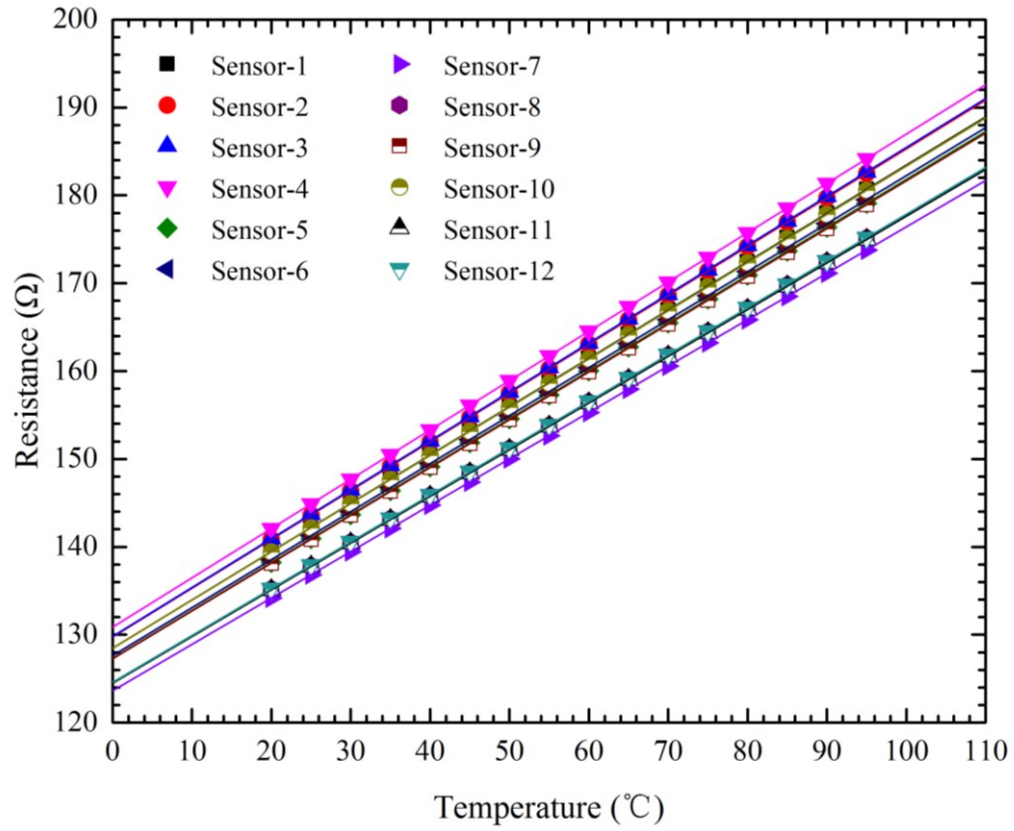


Figure 3. Calibrated curve between the resistance of temperature sensors and the temperature.

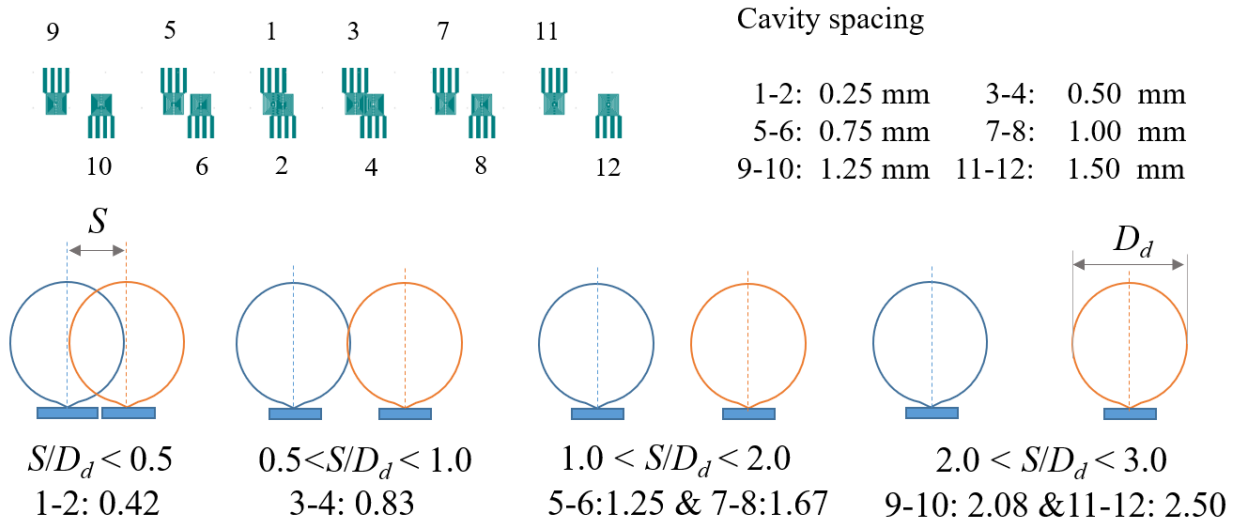


Figure 4. Schematic diagram of cavity spacing, S (mm), dimensionless cavity spacing, S/D_d , and effect on bubble growth.

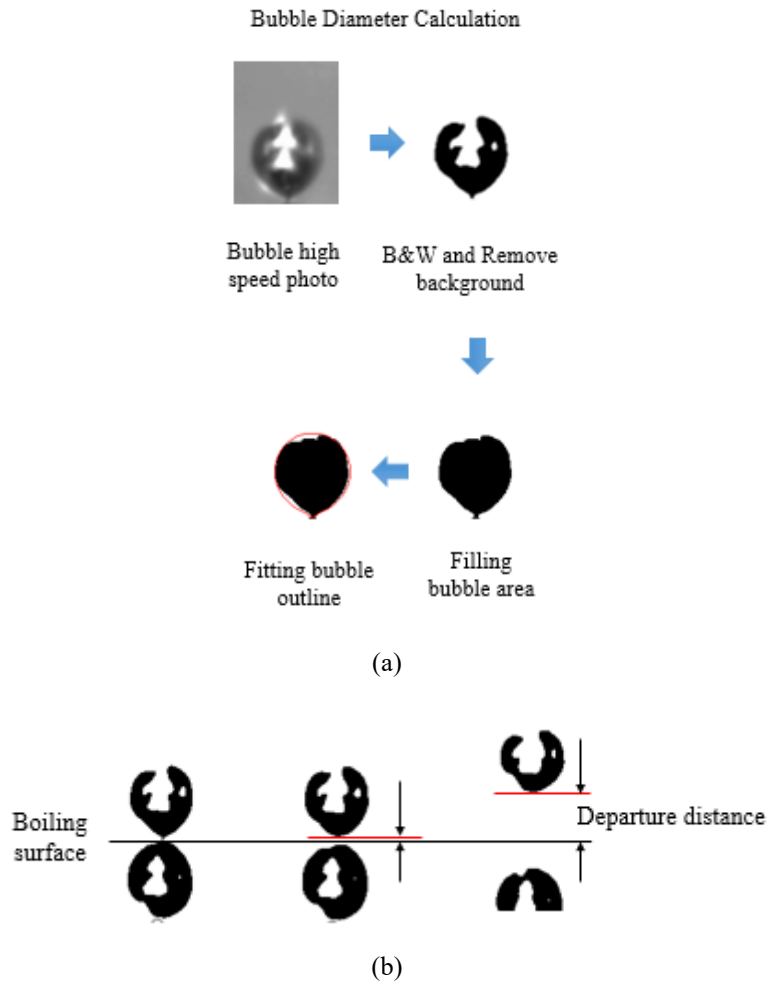


Figure 5. (a) Definition of bubble diameter and (b) definition of bubble departure distance.

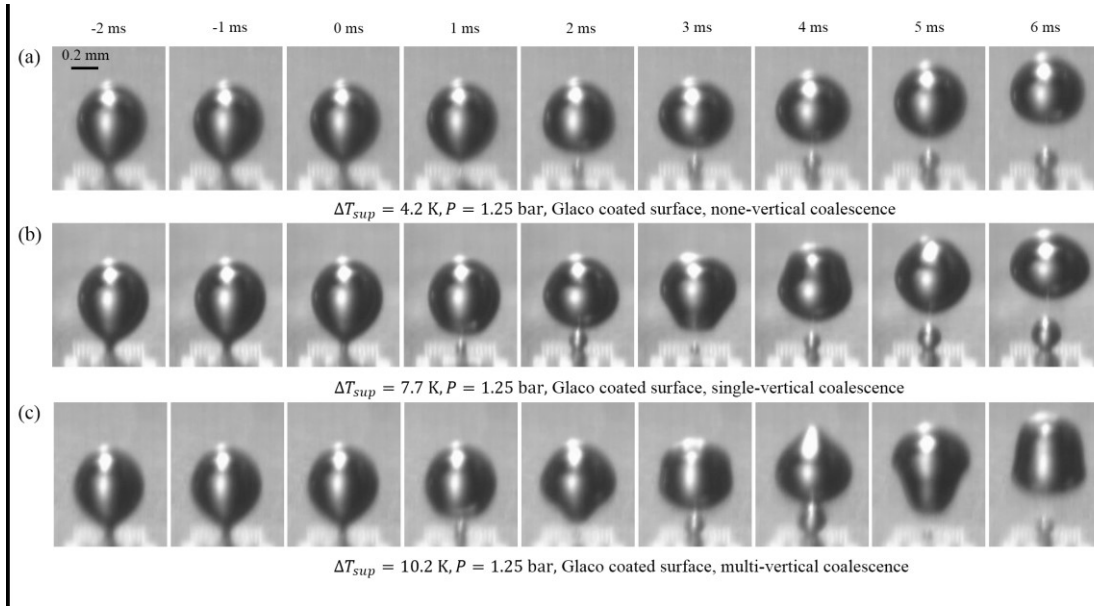


Figure 6. Bubble departure snapshots for different wall superheat degrees with 1.00 mm cavity spacing (a) none-vertical coalescence at $\Delta T_{sup} = 4.2$ K; (b) single-vertical coalescence at $\Delta T_{sup} = 7.7$ K; (c) multi-vertical coalescence at $\Delta T_{sup} = 10.2$ K on Glaco coated surface at 1.25 bar with $t = 0$ ms as the time right before the bubble neck breaks and the first/larger bubble departs.

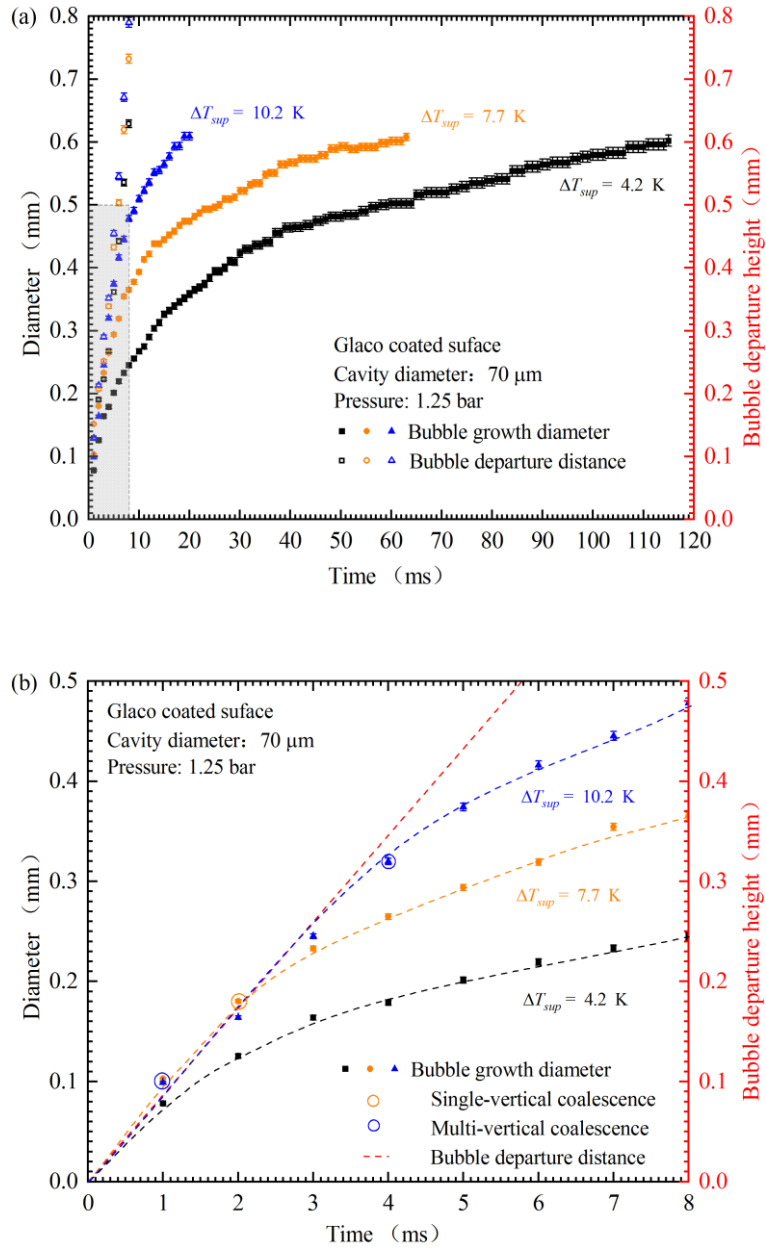


Figure 7. Single bubble growth diameter (mm) and bubble departure distance (mm) versus time (ms) for different superheat degree (K) on Glaco coated surface with 1.00 mm cavity spacing (a) whole period and (b) initial period as the grey area in (a).

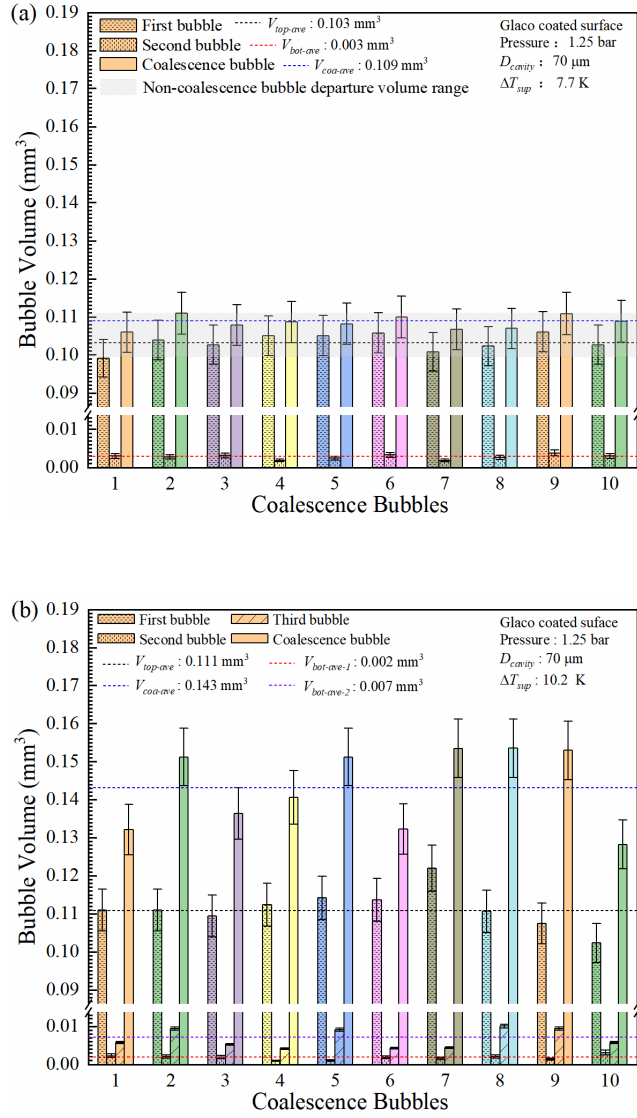


Figure 8. The average bubble volume (mm^3) during (a) single-vertical coalescence of the different bubbles (first/departing, secondary bubble and coalesced bubble) at $\Delta T_{sup} = 7.7$ K and (b) multi-vertical coalescence of the different bubbles (first/departing, secondary bubble, tertiary bubble and coalesced bubble) at $\Delta T_{sup} = 10.2$ K on Glaco coated surface for a total of ten different pairs of bubbles with 1.00 mm cavity spacing.

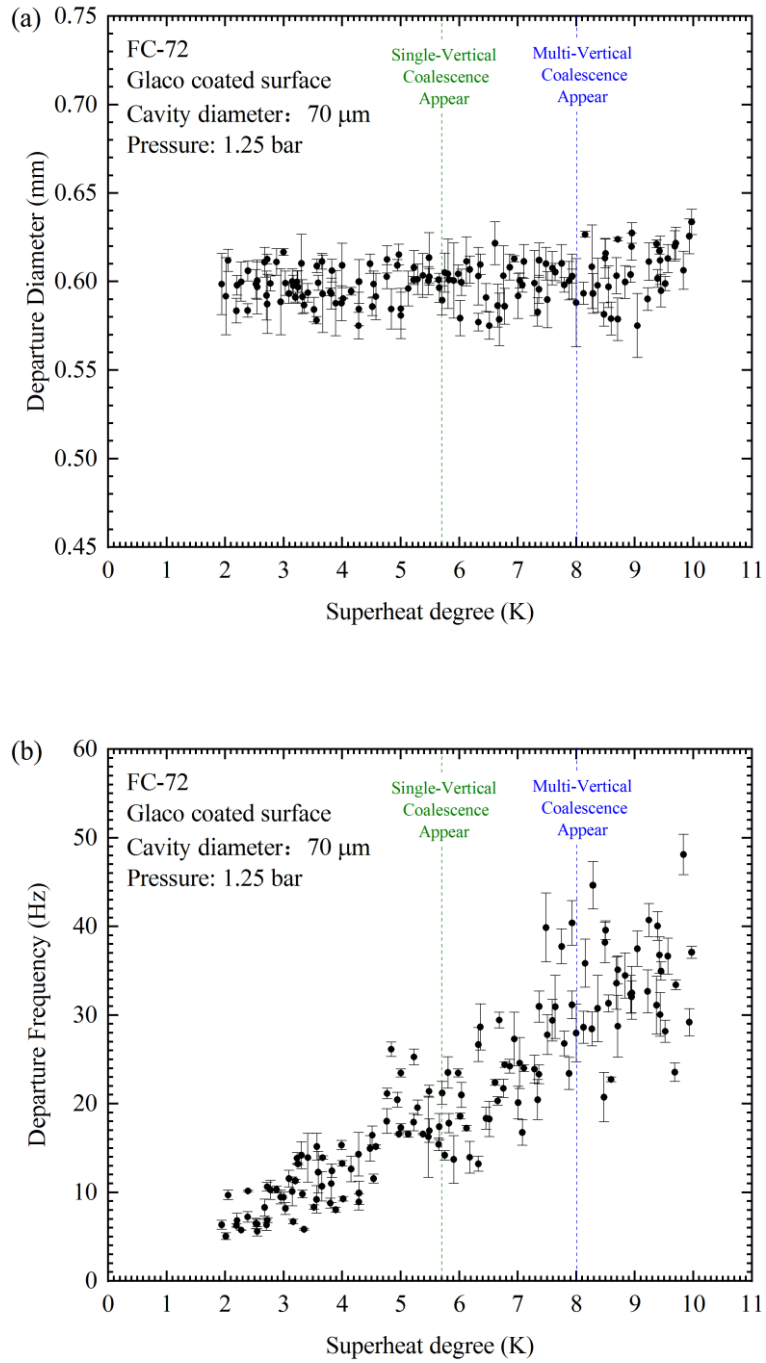


Figure 9. (a) Bubble departure diameter (mm) and (b) bubble departure frequency (Hz) versus superheat degree (K) on Glaco coated surface at 1.25 bar with 1.00 mm to 1.50 mm cavity spacings.

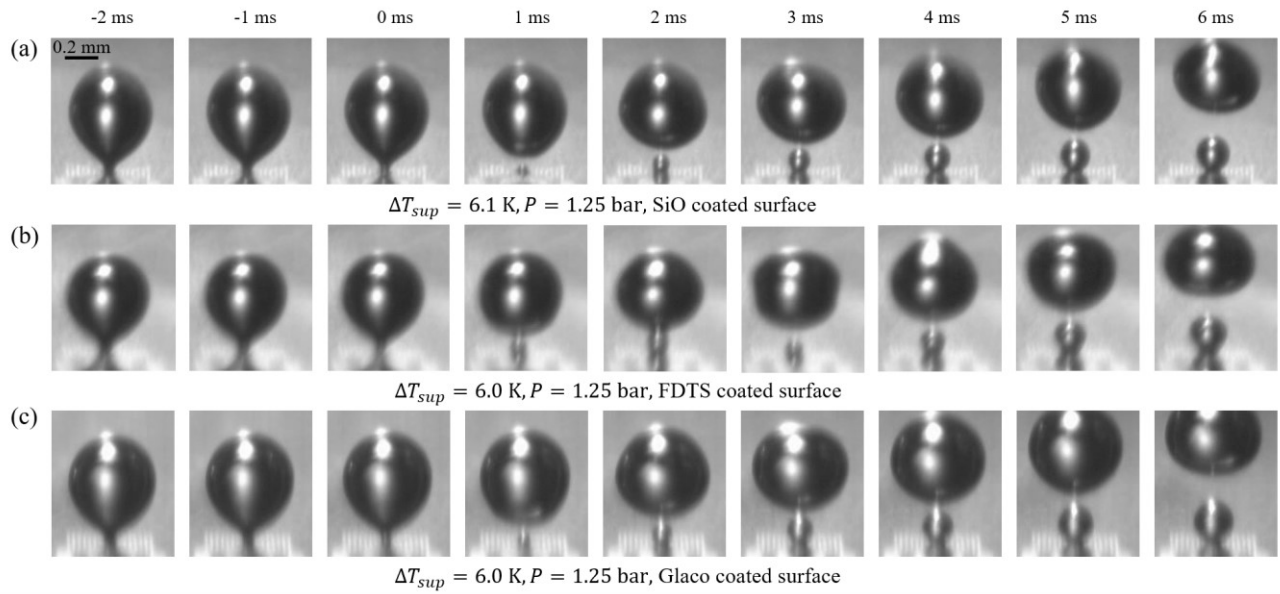


Figure 10. Bubble departure snapshots with different coated surfaces and 1.00 mm cavity spacing.
(6.0 K superheat degree)

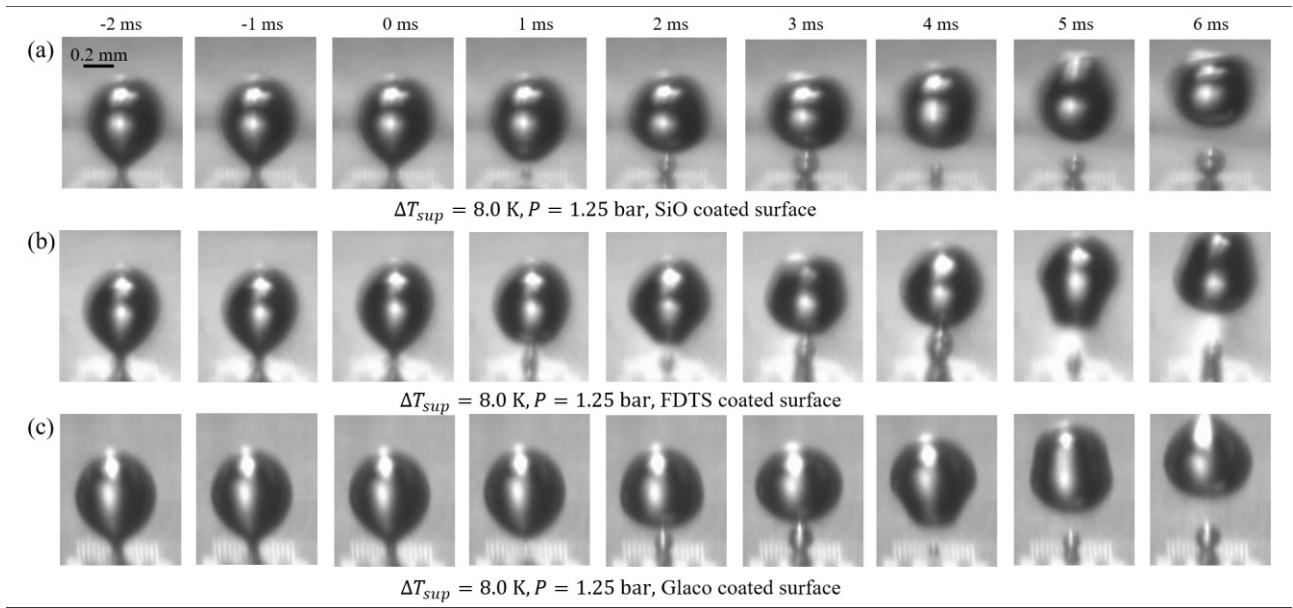


Figure 11. Bubble departure snapshots with different coated surfaces and 1.00 mm cavity spacing (8.0 K superheat degree)

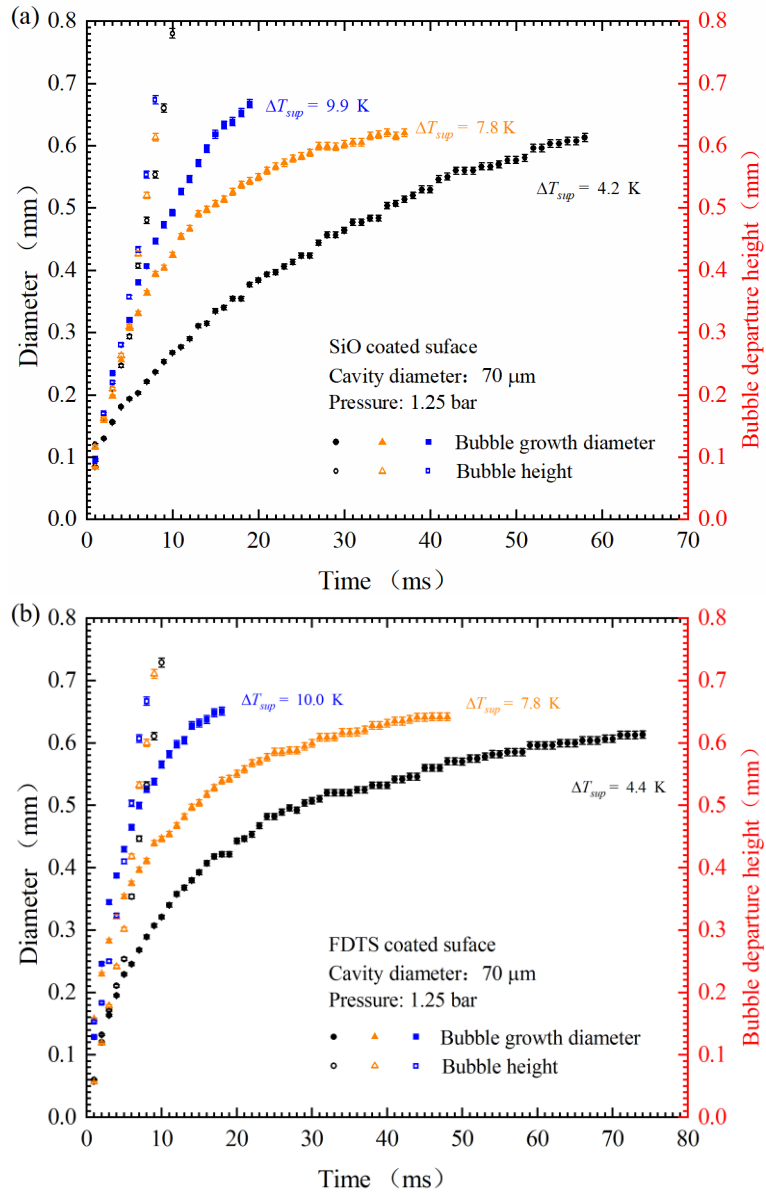


Figure 12. Single bubble growth diameter (mm) and bubble departure height (mm) versus time (ms) with different superheat degree on (a) SiO coated surface and (b) FDTS coated surface with 1.00 mm cavity spacing.

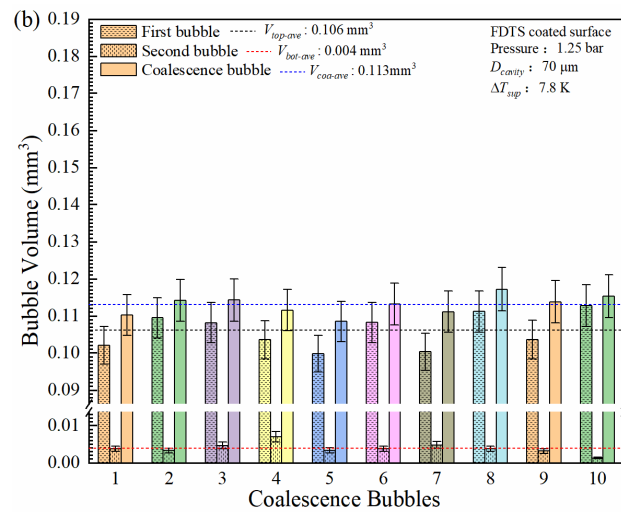
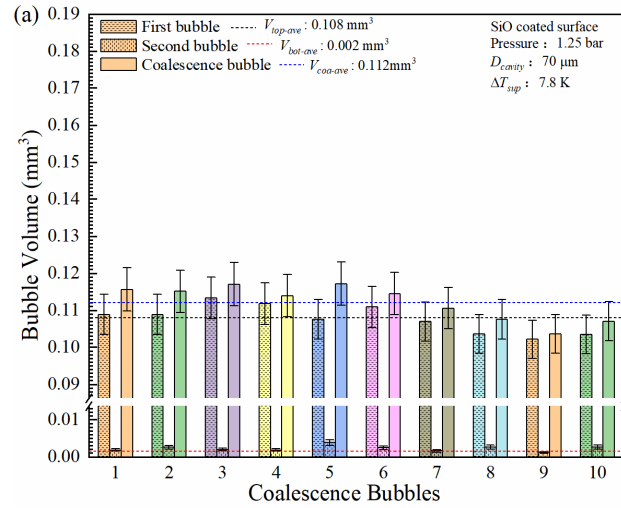


Figure 13. The average bubble volume (mm³) during vertical coalescence of first/departing, secondary bubble and coalesced bubble for a total of ten different pairs of bubbles with 1.00 mm cavity spacing at (a) $\Delta T_{sup} = 7.8$ K on SiO coated surface and (b) $\Delta T_{sup} = 7.8$ K on FDTS coated surface.

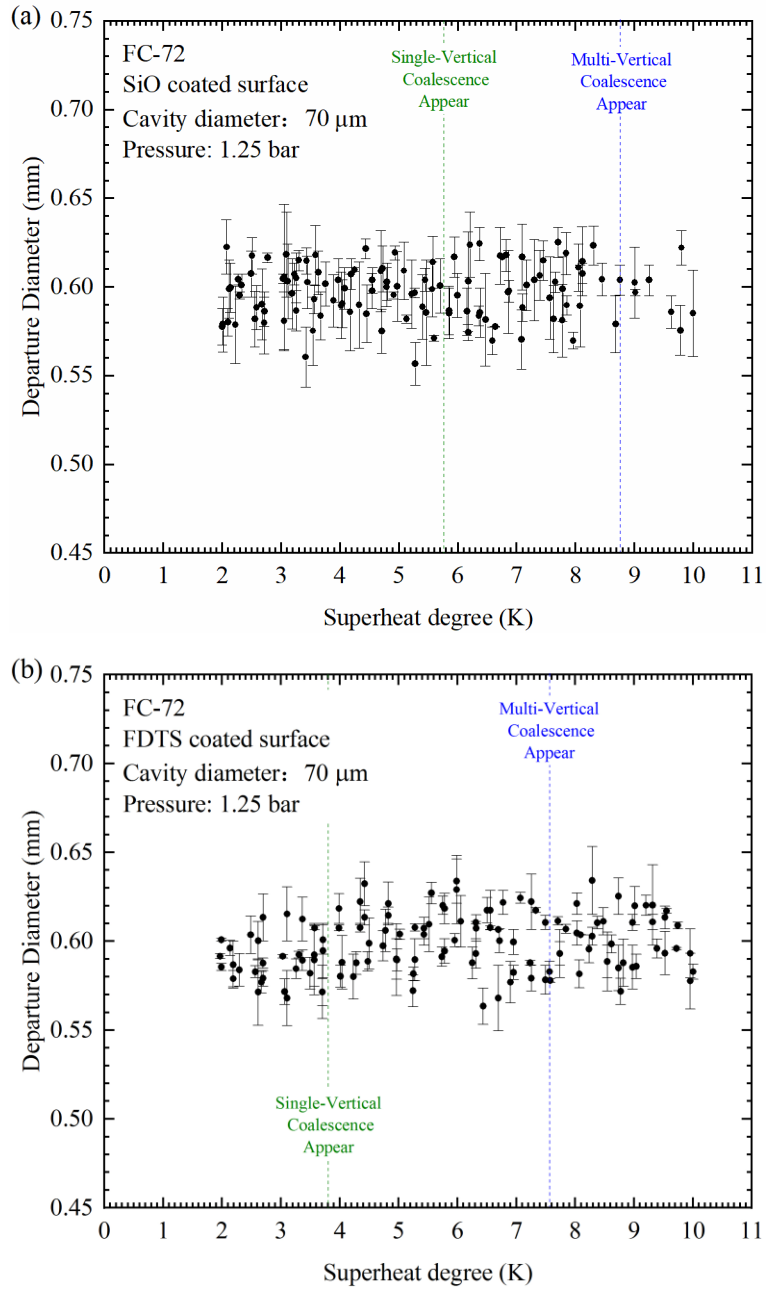


Figure 14. Bubble departure diameter (mm) versus superheat degree (K) with 1.00 mm to 1.50 mm cavity spacings on (a) SiO coated surface and (b) FDTS coated surface.

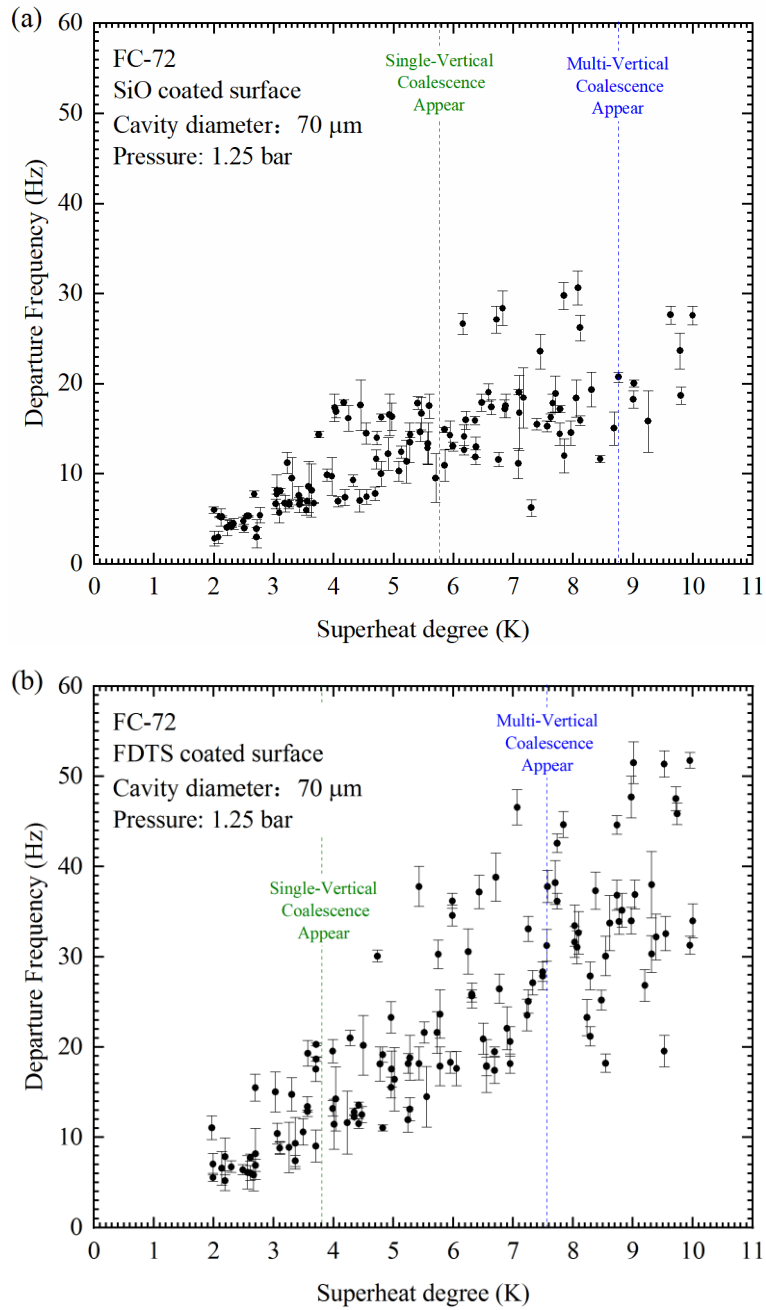


Figure 15. Bubble departure frequency (Hz) versus superheat degree (K) with 1.00 mm to 1.50 mm cavity spacings on (a) SiO coated surface and (b) FDTS coated surface.

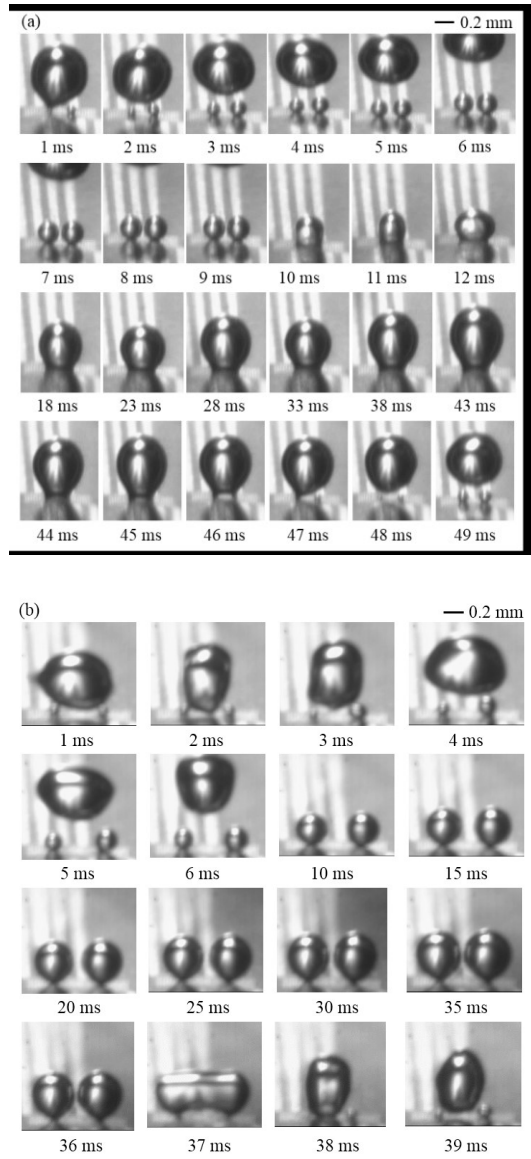


Figure 16. The entire bubble horizontal coalescence cycle on the Glaco coated surface with (a) 0.25 mm cavity spacing and (b) 0.50 mm cavity spacing at approximately 4.7 K superheat degree.

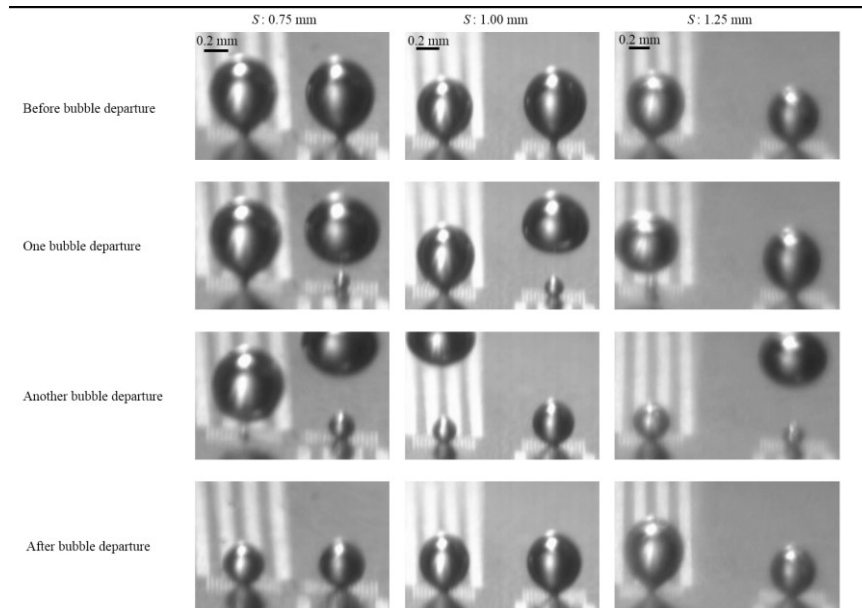


Figure 17. The bubble growth behaviour for 0.75mm, 1.00mm and 1.25 mm cavity spacings on the Glaco coated surface at approximately 4.5 K superheat degree.

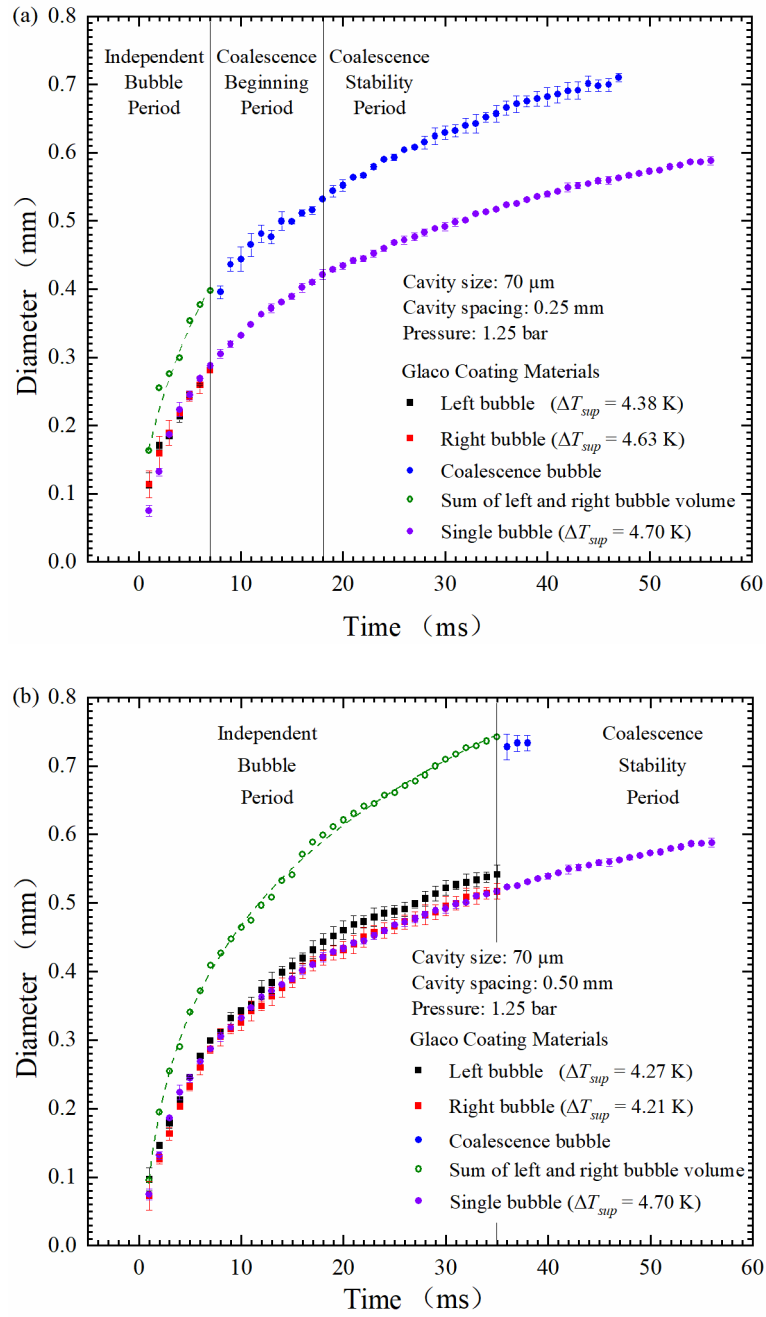


Figure 18. The single and coalesced bubble growth diameter (mm) versus time (ms) for (a) 0.25 mm cavity spacing and (b) 0.50 mm cavity spacing at approximately 4.7 K superheat degree

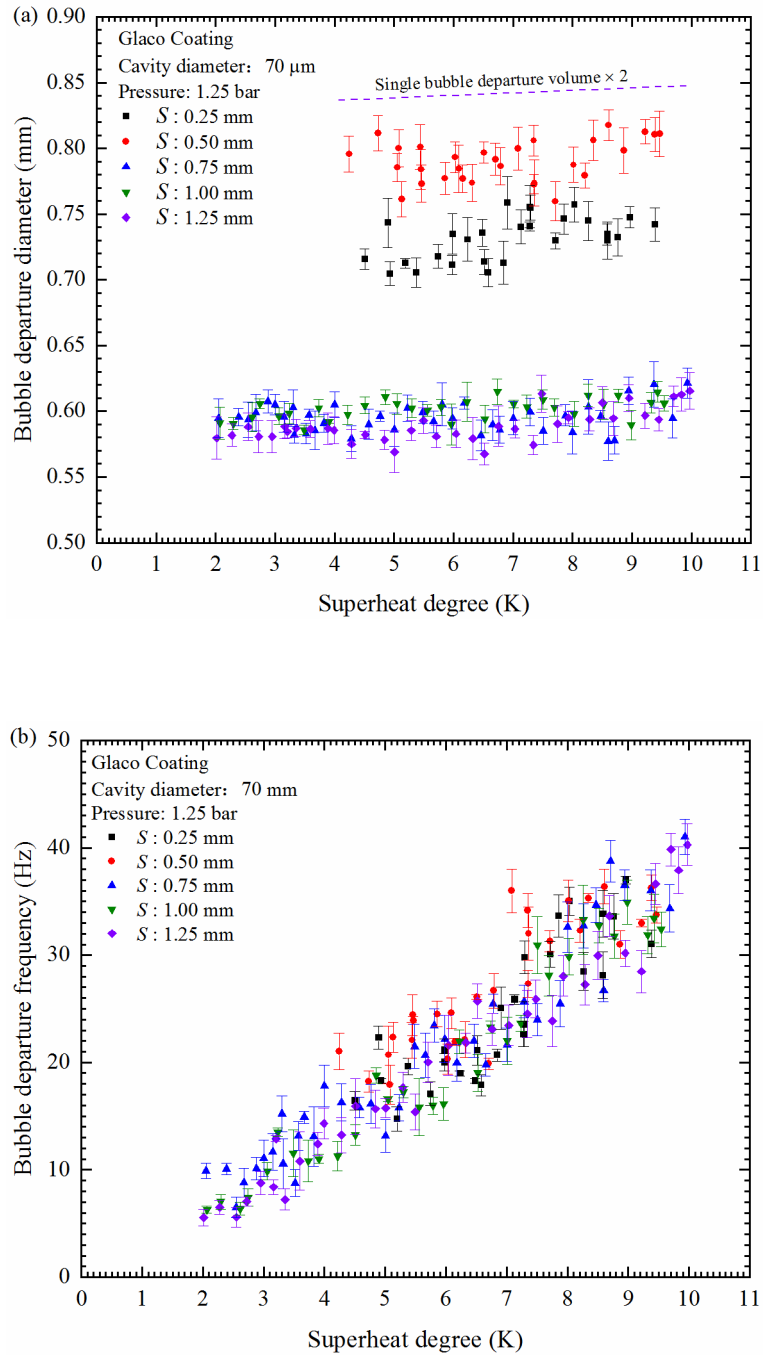


Figure 19. The bubble (a) departure diameter (mm) and (b) departure frequency (Hz) versus superheat degree (K) for different cavity spacings on Glaco coated surface.

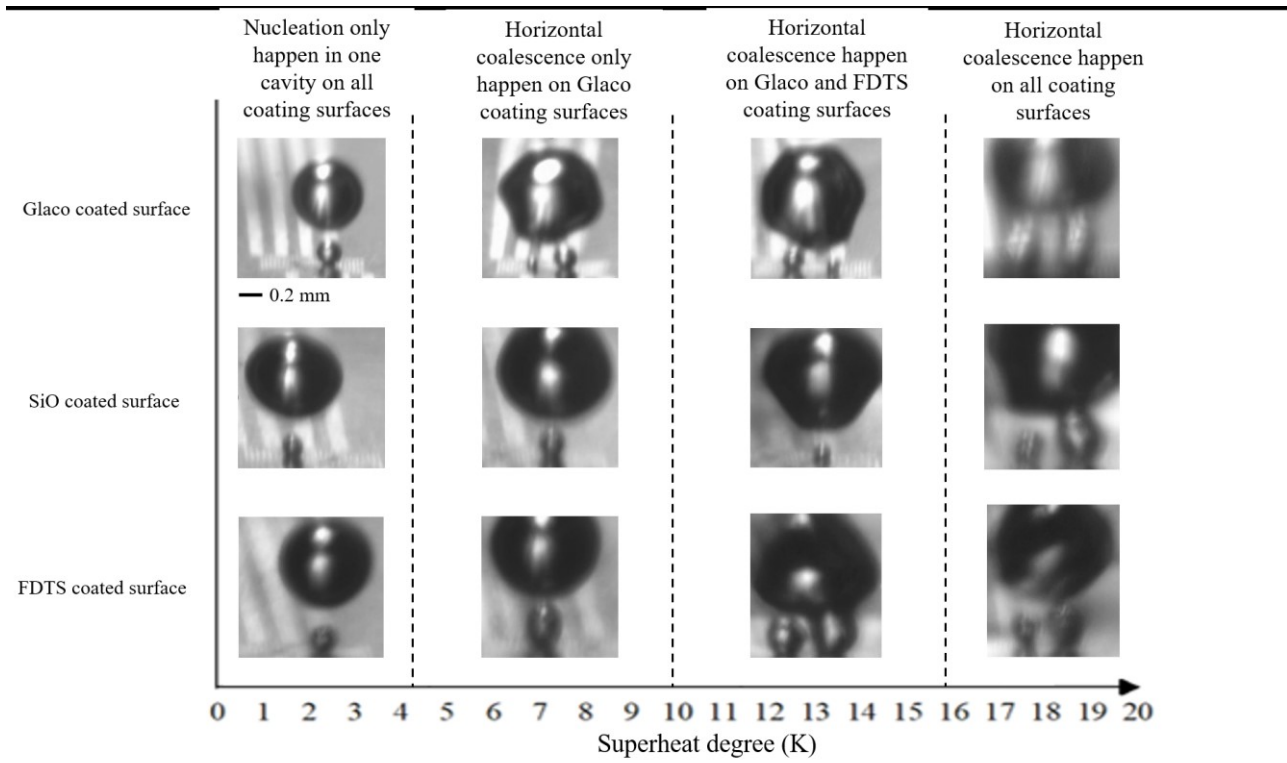


Figure 20. Bubble coalescence performance versus superheat degree (K) and surface coating with 0.25 mm cavity spacing.

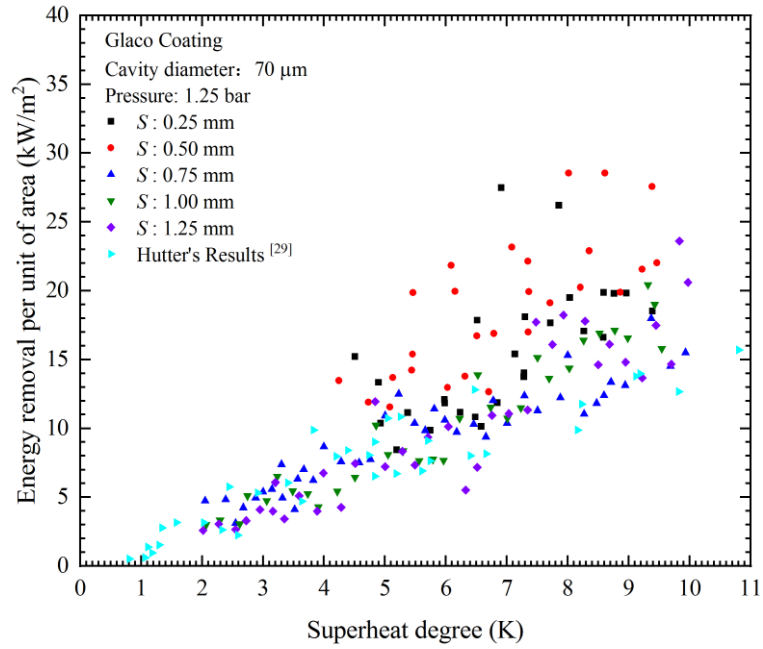
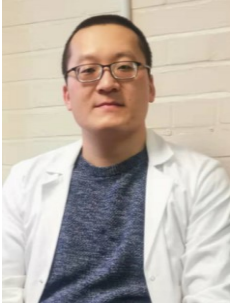


Figure 21. Energy removal per unit of area q_e (kW/m^2) versus superheat degree (K) considering by evaporation.

Notes on contributors



Dr. Jionghui Liu is a Research Associate at the Institute for Multiscale Thermofluids in the School of Engineering, University of Edinburgh. He obtained Ph.D. degree in Power Engineering from Xi'an Jiaotong University. And then he works as a post-doctoral at Queen Mary, University of London (QMUL) on flow boiling and condensation of the mixture in the micro-scale heat exchangers. His current works focused on the phase-change phenomenon and enhance methods in the heat transfer process of thermal management systems.



Daniel Orejon (Dani) is a Senior Lecturer in Chemical Engineering at the Institute for Multiscale Thermofluids at the University of Edinburgh where he investigates the fundamental interactions between liquids and solid surfaces during wetting and phase-change at different scales. He received his Ph.D. degree from the University of Edinburgh in 2013. Dani holds a Visiting Associate Professor at WPI-I2CNER (World Premier International Research Center – International Institute for Carbon-Neutral Energy Research) at Kyushu University Japan since April 2019, an Associate Editorship for the International Journal of Heat and Mass Transfer and a Fellowship of the Higher Education Academy.



Ningxi Zhang is a Ph.D. student at Institute for Multiscale Thermofluids in the School of Engineering, University of Edinburgh. He graduated from University of Glasgow. His research is bubble dynamics on the phase-change phenomenon.



Dr Jonathan G. Terry joined the Institute for Integrated Micro and Nano Systems at the University of Edinburgh in 1999, as a Research Fellow. He is currently the Deputy Head of the Engineering Graduate School and a Senior Lecturer at Edinburgh, where his main area of interest is in the development of More-than-Moore technologies, the integration of novel fabrication processes and materials with foundry CMOS to create smart microsystems.



Anthony J. Walton is Emeritus Professor of Microelectronic Manufacturing with the School of Engineering, University of Edinburgh, U.K. Over the past 25 years, he has been actively involved with the semiconductor industry in a number of areas associated with silicon processing that includes both integrated circuit technology and microsystems. In particular, he has been intimately involved with the development of technologies and their integration with CMOS. He played a key role in setting up the Scottish Microelectronics Centre, which is a purpose-built facility for research and development and commercialization. He has published over 350 papers.



Khellil Sefiane is a Professor of Thermo physical engineering at University of Edinburgh, Associate editor of International Journal of Multiphase Flow and Exxon Mobil Fellow with expertise in novel experimental techniques for heat and mass transfer, phase change, moving contact line, and flow regime transitions in mixture. He received the Institute of Physics Printing & Graphics Science Group Prize for his “Fundamental studies on droplet evaporation”, and elected U.K. representative on EURO THERM committee, member of the Scientific Council of the International Center for Heat and Mass Transfer. He has published more than 230 refereed journal papers.